Efficient megakaryopoiesis and platelet production require phospholipid remodeling and PUFA uptake through CD36

Barrachina, Maria N.; Pernes, Gerard; Becker, Isabelle C.; Allaeys, Isabelle; Hirsch, Thomas I.; Groeneveld, Dafna J.; Khan, Abdullah O.; Freire, Daniela; Guo, Karen; Carminita, Estelle; Morgan, Pooranee K.; Collins, Thomas J. C.; Mellett, Natalie A.; Wei, Zimu; Almazni, Ibrahim; Italiano, Joseph E.; Luyendyk, James; Meikle, Peter J.; Puder, Mark; Morgan, Neil V.

DOI:
10.1038/s44161-023-00305-y

Efficient megakaryopoiesis and platelet production require phospholipid remodeling and PUFA uptake through CD36

Maria N Barrachina[1,2], Gerard Pernes[3], Isabelle C Becker[1,2], Isabelle Allaeys[4], Thomas I. Hirsch[1,2], Dafna J Groeneveld[5], Abdullah O. Khan[6,7], Daniela Freire[1], Karen Guo[1], Estelle Carminita[1,2], Pooranee K Morgan[3], Thomas J. C. Collins[3], Natalie A Mellett[8], Zimu Wei[5], Ibrahim Almazni[6], Joseph E. Italiano[1,2], James Luyendyk[5], Peter J Meikle[8], Mark Puder[1,2], Neil V. Morgan[6], Eric Boilard[4], Andrew J Murphy[3], Kellie R Machlus*[1,2]

[1] Vascular Biology Program, Boston Children's Hospital, Boston, MA, 02115 USA
[2] Harvard Medical School, Department of Surgery, Boston Children's Hospital, Boston, MA, 02115 USA
[3] Haematopoiesis and Leukocyte Biology, Baker Heart and Diabetes Institute, Melbourne, VIC, Australia
[4] Centre de Recherche du CHU de Québec-Université Laval and Centre de Recherche ARThrite, Québec, QC, G1V4G2 Canada
[5] Department of Pathobiology and Diagnostic Investigation, Michigan State University, East Lansing, MI, USA
[6] Institute of Cardiovascular Sciences, College of Medical and Dental Sciences, University of Birmingham, Vincent Drive, Birmingham, U.K, B15 2TT
[7] MRC Weatherall Institute of Molecular Medicine, Radcliffe Department of Medicine and National Institute of Health Research (NIHR) Oxford Biomedical Research Centre, University of Oxford, Oxford, U.K. OX3 9DS
[8] Metabolomics, Baker Heart and Diabetes Institute, Melbourne, VIC, Australia

***Correspondence to:**
Kellie R Machlus
1 Blackfan Circle, Karp 11.214
Boston, MA 02115
Kellie.Machlus@childrens.harvard.edu

Word Count: 4755
Figures: 7
Tables: 1
Extended Data Figures: 7
Extended Data Tables: 2
Supplementary Tables: 2

ABSTRACT

Lipids contribute to hematopoiesis and membrane properties and dynamics; however, little is known about the role of lipids in megakaryopoiesis. Here we show that megakaryocyte progenitors, megakaryocytes, and platelets present a unique lipidome progressively enriched in polyunsaturated fatty acid (PUFA)-containing phospholipids. In vitro, inhibition of both exogenous fatty acid functionalization and uptake, and de novo lipogenesis impaired megakaryocyte differentiation and proplatelet production. In vivo, mice on a high saturated fatty acid diet had significantly lower platelet counts, which was prevented by eating a PUFA-enriched diet. Fatty acid uptake was largely dependent on CD36, and its deletion in mice resulted in low platelets. Moreover, patients with a *CD36* loss-of-function mutation exhibited thrombocytopenia and increased bleeding. Our results suggest that fatty acid uptake and regulation is essential for megakaryocyte maturation and platelet production, and that changes in dietary fatty acids may be a viable target to modulate platelet counts.

EDITOR'S SUMMARY

Barrachina et al. present an extensive lipidomic analysis at different stages of thrombopoiesis and, through in vitro and in vivo experiments, demonstrate that fatty acid uptake, largely dependent on the scavenger receptor CD36, and its regulation are essential for megakaryocyte maturation and platelet production.

Lipids are key for many cell biological processes including membrane construction, organelle compartmentalization, energy storage, and the assembly of signaling effectors.[1] In addition, recent studies have demonstrated a role for lipids in cell fate decisions during hematopoiesis.[2-5] Cells obtain lipids in several ways; essential fatty acids are taken up from the diet (mostly polyunsaturated fatty acids, PUFAs, containing multiple double bonds), while saturated fatty acids (SFAs, no double bonds) can be produced via *de novo* lipogenesis.[6] As such, how lipids are produced and incorporated into cells can be regulated through cellular metabolism and dietary intervention.[5] Megakaryocytes (MKs) are large hematopoietic cells that primarily reside in the bone marrow and produce platelets, which are essential for hemostasis.[7,8] Even though MKs have an extensive, lipid-rich membrane system, the role of lipids in their maturation and during platelet production has not been extensively investigated.

Megakaryopoiesis is the process by which MKs develop from hematopoietic stem cells (HSCs) along the myeloid branch of hematopoiesis under the direction of thrombopoietin (TPO) signaling through its receptor myeloproliferative leukemia virus (MPL). According to the classical model, each mature MK is derived from an HSC that sequentially transitions through the multipotent progenitor (MPP), common myeloid progenitor (CMP), MK-erythroid progenitor (MEP), and MK progenitor (MKP) state.[9] After MKs are terminally differentiated, they undergo maturation[7,8] which includes increasing in size and developing an extensive demarcation membrane system (DMS). The DMS is a highly intertwined membrane network with numerous side branches and multiple connections with the cell surface which serves as the membrane reservoir for proplatelet formation and ultimately becomes the plasma membrane of platelets.[8,10] MKs then extend long proplatelet extensions through endothelial cells and into the vessel lumen and bloodstream, where they rapidly undergo repeated rounds of fission, becoming 1-3 μm circulating platelets.[7,8] The identification of modulators of MK maturation and platelet production is essential, as thrombocytopenia (platelet counts < $150x10^9$/L) can be life-threatening due to a heightened risk of bleeding.[11,12] Current standard of care is limited to therapeutics such as TPO receptor agonists which can have severe side effects including bone marrow fibrosis and leukemic transformation.[13-15] Therefore, there is an urgent need to identify new thrombopoietic agents to increase platelet counts.

Due to the extensive DMS unique to MKs, we postulated that MKs may be more reliant on a particular membrane lipid composition than other cell types. Specifically, the processes of DMS formation and proplatelet production require a profound reorganization of both the MK cytoskeleton and the accompanying membrane system as the DMS folds and then extrudes itself outward and subsequently thins into proplatelet shafts.[7,8] To accomplish this, the MK membrane must acquire the lipids necessary over the course of its maturation to have sufficient flexibility for these processes. Critically, the higher number of double bonds in PUFAs significantly enhance membrane fluidity.[16]

While the function of lipids in platelet production remains ambiguous, recent work has begun to suggest a role for lipids in MK maturation. Valet et al.[17] showed that MKs can take up fatty acids released by adipocytes via CD36 to facilitate their maturation *in vitro*. In addition, Kelly et al. demonstrated that the *de novo* lipogenesis pathway can regulate late-stage MK maturation and platelet formation.[18] These studies support a role for lipids in MK maturation and raise further questions about the relationship between megakaryopoiesis and lipid biosynthesis. Here, we

expand the previously suggested role of lipids in MKs by performing lipidomics to uncover the lipid fingerprint of MEPs, immature and mature MKs, and platelets. We demonstrate that altering both *de novo* lipogenesis and fatty acid functionalization and uptake abrogate megakaryopoiesis and proplatelet formation. Further, we reveal that platelet counts can be modulated *in vivo* by altering dietary fatty acid content. Finally, we identify CD36 as a key fatty acid uptake receptor that affects platelet counts in both mice and humans. These data support a key role for fatty acids in MK maturation and platelet production and suggest that dietary interventions can influence thrombopoiesis.

RESULTS

MKs and platelets display a unique profile enriched in PUFAs

To provide insight into how the cellular lipid profile changes throughout MK differentiation and maturation, we performed a lipidomic study using liquid chromatography tandem-mass spectrometry (LC-MS/MS) starting with MEPs. The indicated cell populations were sorted from adult murine bone marrow and platelets were isolated from autologous blood (Fig. 1a). Dimensionality reduction of all populations revealed that MKs and platelets have a lipidome distinct from their precursor, MEPs (Fig. 1b), which was confirmed when analyzing different lipid class compositions (Extended data Fig. 1a). These data suggest that extensive remodeling of the lipidome occurs during megakaryocyte maturation. Further, when comparing the lipid composition of the microenvironment to the cells that reside in it, such as comparing bone marrow extracellular fluid (BMEF) to bone marrow cells (Extended data Fig. 1b-d) or plasma to platelets (Extended data Fig. 1e), we found that the lipid composition of these cells (Extended data Fig. 1f-i) was unique to their environments. We used a lipid ontology analysis to identify the main lipid species that varied between the different cell populations and found that membrane lipids, glycerophospholipids, and fatty acids were upregulated over the course of megakaryo- and thrombopoiesis (Fig. 1c). This was further supported by analysis of an mRNA sequencing dataset previously published by our group[19] which revealed that MKs are actively regulating key lipid-related mRNAs as they undergo proplatelet formation (Fig. 1d-e), specifically highlighting pathways involved in fatty acid metabolism and uptake. A pathway analysis further emphasized the synthesis of the long chain fatty acyl-CoA and fatty acid metabolism as key pathways involved in proplatelet production (Fig. 1e). Therefore, as lipidomic and mRNA pathway analyses suggested that differences in phospholipids and fatty acids were unique and important to MK maturation and platelet production, we analyzed these lipid classes in our cell populations. Our data revealed that MKs and platelets were enriched in phosphatidylcholine (PC) compared to their progenitors. Conversely, MKs and platelets were reduced in phosphatidylethanolamine (PE), phosphatidylglycerol (PG), and phosphatidylinositol (PI) (Fig. 1f). When examining the differences in the overall fatty acid saturation level, we identified a significant reduction in saturated fatty acids (no double bonds) along the maturation pathway (Fig 1g-h). Notably, we also found that cells acquired increasing levels of more complex PUFA-containing phospholipids (6+ double bonds, Fig. 1g, i) as they matured, with platelets exhibiting the highest levels. This overall pattern of fatty acid remodeling was also seen in other phospholipid classes such as PC, PE, PI, and phosphatidylserine (PS) (Extended data Fig. 1d-g). Taken together, these data reveal significant phospholipid remodeling, and specifically an increase in PUFAs during megakaryopoiesis.

Fatty acids are essential for MK and platelet production

Since we identified that PUFA content increases throughout megakaryopoiesis, we hypothesized that PUFA uptake is important for MK maturation and platelet production. PUFAs are either obtained from the diet and are therefore considered essential fatty acids or are synthesized from essential fatty acid precursors. To test the importance of fatty acid uptake and functionalization in MK differentiation and proplatelet formation, we inhibited ACSL, the enzyme that catalyzes the formation of acyl-CoA from fatty acids, a necessary step for the functionalization of fatty acids and their incorporation into phospholipids (Fig. 2a). We isolated murine bone marrow- (Fig. 2) and fetal liver-derived (Extended data Fig. 2) hematopoietic stem and progenitor cells (HSPCs) and cultured them with TPO for 4 days with the indicated concentrations of the ASCL inhibitor Triacsin C. Inhibition of ACSL led to a significant, dose dependent reduction in the number of immature ($CD41^+$) and mature ($CD41/42^+$) MKs in both bone marrow- (Fig. 2b-c) and fetal liver (Extended data Fig. 2a)-derived MKs.

Next, we inhibited *de novo* lipogenesis using inhibitors of acyl-coA carboxylase (ACC, PF-05175175) and fatty acid synthetase (FASN, Cerulenin) (Fig. 2d). Both inhibitors significantly and dose dependently reduced MK maturation in bone marrow- (Fig. 2e-f) and fetal liver-derived (Extended data Fig. 2 c-d) MKs. Notably, the frequency of mature MKs ($CD41/42^+$) was decreased more than immature MKs ($CD41^+$). None of the inhibitors were cytotoxic (Extended data Fig. 2b, d, f), suggesting that the effects on HSPCs were due to a failure in MK differentiation and not cell death.

Once mature, MKs remodel their DMS into proplatelets. We postulated that this process is dependent on a highly specific membrane lipid content to allow for proplatelet elaboration. To explore the role of fatty acid uptake/functionalization and synthesis on proplatelet formation, we treated mature MKs (day 4 of culture, i.e. 24h preceding proplatelet formation) with the indicated inhibitors and monitored proplatelet formation over 24 hours (Fig. 2g). Triacsin C treatment resulted in a significant reduction in both the number of MKs making proplatelets and the area of formed proplatelets (Fig. 2h-j), suggesting a severe impairment in proplatelet elaboration. However, neither of the *de novo* lipogenesis inhibitors significantly impacted proplatelet formation (Fig. 2k-n), indicating that *de novo* lipogenesis may not be essential for proplatelet generation. To exclude the possibility that effects on proplatelet formation were due to impaired mitochondrial activity, we measured oxygen consumption rate using a Seahorse mitostress assay of murine bone marrow-derived MKs treated with the indicated inhibitors. The MK mitochondrial profile was not altered upon inhibition of fatty acid synthesis with Triacsin C, Cerulenin, or PF-051751 (Extended data Fig. 2g-h), supporting our conclusion that the observed changes in MK maturation and/or proplatelet formation were due to a role of fatty acids in membrane incorporation and not mitochondrial metabolism. Together, these data suggest that MK differentiation and maturation are reliant on both fatty acid uptake and *de novo* lipogenesis. However, proplatelet formation appears uniquely reliant on fatty acid uptake and functionalization.

SFA-enriched high fat diet reduces platelet counts

Our data demonstrated that megakaryopoiesis and platelet production are dependent on fatty acid uptake, functionalization, and metabolism. We therefore postulated that altering the

exogenous supply of fatty acids will alter MK phenotype and subsequent platelet production. We first wanted to examine the effects of direct supplementation of SFAs on MK development and platelet production. To confirm and visualize SFA incorporation into MKs in vitro, we performed click-chemistry using palmitic acid modified with a terminal alkyne group. First, HSPCs isolated from murine bone marrow were supplemented with modified SFA in culture. After 4 days, mature MKs were functionalized with an azide-linked fluorescent reporter, which bound modified palmitic acid in the MK membrane (Fig. 3a), allowing its visualization (Fig. 3b). We observed a robust, dose-dependent incorporation of palmitic acid throughout the plasma and demarcation membranes of MKs (Fig. 3b-c). Additionally, MKs supplemented with palmitic acid were significantly larger and displayed a reduced capacity to form proplatelets in vitro (Fig. 3d-e). These data confirmed that MKs incorporated SFAs (palmitic acid) into their membrane as they differentiate and mature, resulting in increased size and decreased proplatelet generation.

To test the impact of an SFA-enriched diet in vivo, male mice were fed a 60% high fat diet (diet-induced obesity (DIO) model) for 14 weeks (Fig. 3f), which led to increased body weight (Fig. 3g). To determine whether this high fat diet affected HSPC differentiation, we quantified the number of bone marrow HSPCs by flow cytometry. While we did not detect differences between long term (LT)-HSC, Pre-GM, or Pre-MK populations after 14 weeks, we found a significant increase in short-term (ST)-HSCs and Pre-MKs (Fig. 3h). Further, bone marrow MKs were significantly larger in DIO mice (Fig. 3i-j), consistent with our in vitro data (Fig. 3d), while their numbers were unchanged. Finally, platelet counts were significantly reduced after administration of the SFA-enriched diet (Fig. 3k). No significant differences were found in other blood parameters (Extended data Fig. 3a-e). To confirm that the reduction in platelet counts was not due to differences in platelet clearance, we performed an in vivo platelet lifespan assay and found no differences between the DIO and control mice (Extended data Fig. 3f). These data revealed that enriched dietary SFAs increased MK size and decreased platelet production both in vitro and in vivo. Further, these data support our hypothesis that enhanced membrane PUFA content is necessary for maximal proplatelet production, and that interruption of this process through increased dietary SFA abrogates platelet production.

PUFA-enriched high fat diet prevents platelet reduction

Feeding mice a high fat diet with an enrichment in SFA resulted in decreased platelet counts. This is consistent with our lipidomic data, which revealed a clear bias towards PUFAs, and not SFAs, during thrombopoiesis. Thus, we hypothesized that substituting the SFAs for PUFAs in the high fat diet may prevent obese mice from having reduced platelet counts. To explore this, we first established whether MKs could take up PUFAs, and examined their effect *in vitro* by performing click chemistry as described above. Indeed, MKs dose-dependently incorporated arachidonic acid (Fig. 4a), however it did not significantly alter their area (Fig. 4b) or capacity to form proplatelets in vitro (Fig. 4c).

To determine whether the low platelet counts observed in the DIO model were a consequence of the high fat diet or the fatty acid saturation status (high SFA), we fed male mice a matched 60% high fat diet enriched in PUFAs (Fig. 4d) instead of SFAs. Mice fed the PUFA diet weighed significantly more than controls (Fig. 4e), but glucose levels were indistinguishable (Fig. 4f). Mice

on the high PUFA diet had significantly increased platelet counts after 4 weeks, and platelet counts remained elevated at the study endpoint (Fig. 4g-h). No differences were found in other blood parameters (Extended data Fig. 4a-c) and plasma TPO levels of all mice were within the normal range (Extended Data Table 1). Moreover, there were no differences in platelet lifespan between mice fed chow versus the PUFA-enriched diet (Extended data Fig. 4d).

In addition, when assessing the amount of circulating, newly generated reticulated platelets using thiazole orange, we found that mice fed the enriched PUFA diet had a tendency toward more immature platelets in circulation (Fig. 4i-j). Comparable to the DIO mice, MKs in the PUFA-fed mice were significantly larger than the chow group while their number remained unaltered (Fig. 4k-l). In addition, their maturation, as measured by ploidy, was substantially enhanced, with a significant decrease in the number of 16n MKs and an increase in 32n MKs (Fig. 4m), suggesting an overall shift to higher ploidy. Together, these data reveal that enhancing the amount of PUFAs in the high fat diet can rescue the reduced platelet counts seen in the DIO model. These results underscore the role of dietary PUFAs in contributing to MK maturation and reveal that supplementation with PUFAs can enhance MK maturation and platelet production.

Platelets are unchanged in *Cd36*$^{-/-}$ mice fed high fat diets

Our data revealed that MKs and their progenitors readily take up exogenous fatty acids, and this is an important process during their maturation. Further, modifying dietary fatty acids can directly impact platelet counts in vivo. As such, identification of a receptor responsible for fatty acid uptake in MKs and their progenitors is key in understanding the mechanism of how fatty acids impact megakaryopoiesis. As Valet et al. recently demonstrated that MKs can take up fatty acids via the scavenger receptor CD36 to help facilitate membrane maturation[17], and CD36 was upregulated in proplatelet-forming MKs (Fig. 1e), we explored whether CD36 was the mechanism by which MKs and their progenitors incorporate exogenous fatty acids. We utilized a mouse model constitutively lacking CD36 (*Cd36*$^{-/-}$).[20] *Cd36*$^{-/-}$ mice exhibited significantly reduced platelet counts (Fig. 5a).[17] While MPV and IPF remained unchanged, red blood cell counts were also significantly reduced (Fig. 5b). To directly test if CD36-deficient MKs had a defect in taking up fatty acids in vitro, we used click-chemistry on MKs from *Cd36*$^{-/-}$ and wildtype mice cultured with either the SFA palmitic acid (Fig. 5c-d) or the PUFA arachidonic acid (Fig. 5e). In line with our hypothesis, *Cd36*$^{-/-}$ MKs took up significantly less fatty acids (Fig. 5c), suggesting that the CD36 receptor plays a substantial role in fatty acid uptake of both SFAs (Fig. 5d) and PUFAs (Fig. 5e) in MKs.

We next cultured HSPCs derived from *Cd36*$^{-/-}$ and wildtype mice and found a significant decrease in the number of mature MKs that differentiated from HSPCs from *Cd36*$^{-/-}$ mice, suggesting that fatty acid uptake through CD36 is important not only for platelet production but also MK differentiation (Fig. 5f). We examined the number and area of CD41+ cells in *Cd36*$^{-/-}$ bone marrow and found no significant reduction (Fig. 5g). Moreover, the ploidy of in vitro differentiated MKs was largely unchanged, with only a decrease in the 2n population (Fig. 5h). As *in vitro* MK differentiation was affected in *Cd36*$^{-/-}$ mice, we next characterized proplatelet formation. Critically, CD36-deficient MKs displayed a notable defect in proplatelet formation with both the number of MKs forming proplatelets and proplatelet area being significantly reduced (Fig. 5i-j). This finding strongly suggests that proplatelet formation is dependent on the uptake of essential fatty acids

(PUFAS) through CD36. Together, these data indicate that loss of MK CD36 decreases the uptake of both SFAs and PUFAs into MKs in vitro. Further, lack of CD36 on HSPCs decreases their ability to differentiate into MKs and the capacity of MKs to make proplatelets.

If CD36 is the receptor that facilitates uptake of fatty acids into MKs and their progenitors in vivo, then mice lacking this receptor would have MKs that are resistant to alterations in dietary fatty acids. Therefore, to test whether the loss of CD36 *in vivo* could disrupt the ability of both SFA- and PUFA-enriched high fat diets to modulate platelet counts, we fed mice chow or 60% high fat diets enriched in either SFAs (DIO model) or PUFAs. Notably, there were no significant differences in platelet counts or platelet production across the mice fed the three different diets after 8 and 13 weeks (Fig. 6 a-f). At week 13, we examined the CD41+ cells in the bone marrow of *Cd36*$^{-/-}$ mice on all diets and found no significant alterations in either MK number or size, consistent with the lack of change in platelet counts (Fig. 6 g-i). This suggests that loss of CD36 abrogated the ability of dietary fatty acids to alter MK phenotype and platelet counts in vivo. Together, these data further support the role of CD36 as a key receptor that takes up dietary fatty acids that drive MK maturation and platelet production.

Patients with a familial *CD36* mutation have thrombocytopenia

To substantiate the biological relevance of CD36 function in platelet production in humans, we identified a family with an idiopathic thrombocytopenia; patients II.1 and II.2 were recruited to the UK-GAPP study (Fig. 7a, Extended data Fig. 6), and clinical histories evaluated. Whole blood cells counts were taken, revealing low platelet counts and high MPV and IPF values (Fig. 7b, Table 1). In addition, the mother (I:2) had bleeding episodes and low platelet counts. Whole Exome Sequencing (WES) analysis was performed on the two patients using a bioinformatic pipeline workflow which identified an average total of 43,884 variants. Genetic variants were filtered against a panel of 358 genes known or predicted to be associated with platelet count, function, or lifespan. These variants where then filtered out by excluding all synonymous and intronic variants followed by excluding all variants with a MAF > 0.01 (Fig. 7c). Pathogenicity prediction of the variants were determined by utilizing the prediction tools (Mutation Taster, PolyPhen-2, SIFT, Provean) and the variants were classified based on the ACMG guidelines. Plausible candidate variants in each patient were then selected based on the pathogenicity prediction (Fig. 7d). A detailed schematic outlining this workflow can be found in Extended data Fig. 6. In both patients II.1 and II.2, we identified a pathogenic heterozygous stop gain variant in exon 10 of the CD36 gene (c.975T>G; p. Tyr325Ter, Fig. 7c).

Although this variant has previously been reported at a relatively high frequency (0.08929) in the Afro-Caribbean population compared to the overall population (8.33e-3) and linked to thrombocytopenia[21], it has not been functionally characterized. Therefore, the relationship between the receptor function and the reported patient phenotype could not be directly discerned. The c.975T>G; p. Tyr325Ter variant was predicted to encode a truncated CD36 protein which lacked the carboxyl-terminal transmembrane domain and potential function of the CD36 protein. Fittingly, western blotting analysis using platelet lysates from the *CD36*-mutation positive patients revealed a truncated band (Fig. 7e). Of note, the tyrosine residue at position 325 is highly conserved across multiple species (Fig. 7f). We modelled the predicted structure of the CD36

ectodomain using homology modelling based on Fu-Lien et al.[22], showing the absence of a significant portion of the WT CD36 protein as a result of the *CD36* nonsense variant, leading to the truncation and significant loss of domains crucial to the normal functioning of CD36 (Fig. 7g-h). Together, these modeling and experimental data supported the conclusion that the c.975T>G; p. Tyr325Ter mutation led to a truncation of the CD36 protein.

We further investigated the function of the CD36 mutant by generating constructs and cloning the wildtype *CD36* cDNA into a pEF-BOS expression vector followed by site-directed mutagenesis to generate 2 mutant forms of CD36: (i) a deletion of the amino acids following the nonsense variant (Tyr325Ter) to the stop codon of the mature protein at amino acid residue 472 and (ii) a substitution of the point mutation only (c.975T>G, p.Tyr325Ter). Initially, the expression of the 3 constructs was measured and validated using western blotting, confirming the truncation effect of the 2 mutant CD36 proteins in both Jurkat T cells and HEK293 cells (Fig. 7i). Flow cytometry was then used to probe the expression of CD36 mutant proteins on the cell surface. Of note, only wildtype CD36 and not the mutant constructs, was detected (Extended data Fig. 5a), suggesting that the other constructs were not trafficked to the cell surface. Next, we studied the signaling capacity of the CD36 constructs using a nuclear factor of activated T cells (NFAT)-luciferase reporter assay. The CD36 wildtype protein robustly activated the NFAT-luciferase, while the mutant protein did not, confirming the absence of signaling capacity for the CD36 mutants (Fig. 7j). These data are consistent with the flow cytometry data and demonstrate that the mutant CD36 protein indeed does not reach the cell surface and does not signal, conferring a complete loss of function in the reported mutation. Together, our data reveal that in both humans and mice, loss of CD36 function results in reduced platelet counts, underscoring its importance in efficient platelet production.

Discussion

Through lipidomic analyses, we uncovered an enrichment in PUFAs, essential fatty acids that are primarily diet-derived, throughout MK differentiation and maturation and platelet production. Our data then revealed that fatty acid uptake, functionalization, and metabolism play differing but essential roles in MK differentiation and proplatelet production. Specifically, platelet production from MKs can be modified both in vitro and in vivo by varying the availability of exogenous PUFAs. We demonstrated that CD36 is a key receptor responsible for the uptake of fatty acids in MK progenitors. We further report that a familial loss-of-function mutation in *CD36* results in thrombocytopenia, suggesting that lipid uptake plays a critical role in platelet production.

Lipids are a vast class of biomolecules which fulfill three general functions: energy, membrane structure, and signaling.[4,5] To date, an impressive amount of experimental data has given insights into membrane biogenesis as well as homeostasis and lipid-protein interactions, which paves the way for targeted modification of membrane lipid compositions.[23] In 1987, Dio et al. showed that adding SFAs (palmitic acid, etc.) to a murine fibroblast cell line results in a severe inhibition of cell growth.[24] In contrast, increasing the PUFA concentration in liposomes results in a more flexible plasma membrane with a higher deformation rate in response to applied force.[25] The idea of enhancing membrane flexibility by modulating PUFA content was further substantiated by Manni et al.[16] Their study revealed that increasing the PUFA content in liposomes results in a higher

tubulation rate. This process bears a striking resemblance to proplatelet production, which requires reorganization of the MK membrane system. Our data showed that increasing the dietary SFA:PUFA ratio resulted in a reduction in platelet generation both in vitro and in vivo. One way by which increased SFAs may be reducing proplatelet production is through creating a membrane that is too rigid to accommodate proplatelet extension. Conversely, replacing SFAs with PUFAs may ensure that the MK membrane is sufficiently flexible to allow for both DMS formation and proplatelet production. This is consistent with our lipidomic analysis revealing that MKs and platelets were increasingly enriched in PUFAs. These results highlight the potential to manipulate dietary fatty acid ratios and thereby modify MK phenotype and increase or decrease platelet production in vivo. Ultimately, these approaches may be able to fulfill a significant unmet clinical need by providing ways to modulate thrombopoiesis and mitigate abnormal platelet counts.

Changes in exogenous lipid availability and content are associated with a variety of diseases including obesity, which has become a significant health problem worldwide.[26] Previous studies have demonstrated that alterations in lipid metabolism and changes in plasma lipid profile are associated with the onset and progression of obesity-related complications.[27] Often, however, obesity is associated with a pro-inflammatory and/or pro-thrombotic state that enhances the risk of developing cardiovascular diseases, where platelets play a well-established pathogenic role.[28-30] In these settings, it is challenging to study the impact of obesity and an altered plasma lipid profile on MKs and platelets independent of comorbidities such as inflammation.[31,32] Recently, a new subset of obese individuals classified as ‘metabolically healthy obese' (MHO) were found to be protected against worsening metabolic health.[33,34] Despite the debate about the use and clinical implications of MHO as a diagnosis, obesity without cardiometabolic abnormalities may provide a unique human model system to study mechanisms linking different diets and fat accumulation to obesity-related cardiometabolic complications.[33] To date, no studies have reported how MHO may impact megakaryopoiesis or platelet production in humans. However, our in vitro data suggest that changes in plasma lipid content alone may lead to changes in MK maturation and platelet production, even in the absence of inflammation or other comorbidities associated with obesity. Notably, depending on the lipid profile, our data suggest that these changes may not always be pathogenic. Further, these data set the stage for future studies examining how changes in dietary lipids might also modify platelet function and reactivity.

CD36 is a multifunctional protein; one of its roles is to accelerate exogenous fatty acid uptake and incorporation into more complex lipids.[35,36] Here, we substantiated CD36 as a key receptor for the uptake of fatty acids in MKs and their progenitors and revealed that loss of CD36 led to reduced platelet counts in both mice and humans. These findings align with recent studies that demonstrate fatty acid uptake transfer between adipocytes and MKs is dependent on CD36.[17] Notably, evidence suggests that there is little expression of CD36 on HSCs, but expression increases dramatically in MKs[37], providing a possible mechanism for how they rapidly accumulate fatty acids over maturation via a cell intrinsic manner.

There are also important limitations to this work that should be noted. First, our lipidomic results reflect total lipids, and membrane lipids do not distinguish between the plasma/demarcation membrane and organelle membranes. Additionally, we only identified and characterized two patients with the c.975T>G, p.Tyr325Ter *CD36* mutation. There have been various *CD36* mutations identified, some of which have been associated with thrombocytopenia.[21,38] Notably,

many of these mutations have not been functionally characterized, making their relationship with platelet counts hard to interpret because it is unknown how each mutation affects CD36 receptor activity. In addition, the fact that *Cd36*$^{-/-}$ mice and humans with mutated or absent CD36 have both MKs and platelets, albeit at reduced levels, suggests that other receptors, such as the free fatty acid receptors (FFARs) are also involved in fatty acid uptake.[39] Specifically, $FFAR_2$ may be a plausible candidate as it is expressed in MKs and their precursor cells.[40]

In summary, our data provide unique insights into the functional role of lipids, diet, and lipid metabolism during MK differentiation, maturation, and platelet production. We have further validated an essential receptor, CD36, as a key mechanism for lipid uptake and identified a *CD36* mutation that is a genetic determinant of thrombocytopenia and pathological bleeding. In the future, we aim to identify additional MK-specific lipid signatures to determine different ways to increase or decrease megakaryopoiesis and platelet production. This could be as simple as altering fatty acid ratios in the diet or involve therapeutics that target key fatty acid biosynthesis enzymes or the uptake receptor CD36. Ultimately, these approaches may be able to meet a significant unmet clinical need in the modulation of thrombopoiesis to mitigate abnormal platelet counts.

Methods

Animal Models

CD-1 and C57BL/6J mice were acquired from Charles River Laboratories (Worcester, MA) or The Jackson Laboratory (Bar Harbor, ME). Mice were housed in the animal facilities at Boston Children's Hospital, Boston, MA or Michigan State University, East Lansing, MI. All animal work was approved by the international animal care and use committee at Boston Children's Hospital, Boston, MA (Protocols 00001248 and 00001423) and Michigan State University (PROTO201800186). In all terminal experiments, mice were sacrificed using methods consistent with IACUC protocol guidelines.

For experiments with high fat diets, adult C57BL/6J and *Cd36*$^{-/-}$ mice were placed on the following diets: 1) Research diets Inc. D12492, Rodent Diet With 60 kcal% from fat and 2) Research diets Inc. D22050406i, Rodent Diet with 60 Kcal% Fat enriched in polyunsaturated fatty acids. As a control, mice were fed a chow diet (D12450B, Research diets Inc.). Mice received water and food ad libitum. Mice were sacrificed at the indicated endpoints using methods consistent with IACUC protocol guidelines. *Cd36* knockout mice (*Cd36*$^{-/-}$) were obtained from The Jackson Laboratory (Strain #019006). Homozygous mice were bred to maintain a colony of knockout mice. Ear clipping specimens were sent to Transnetyx, Inc for genotyping to ensure integrity of the strain and preservation of the *Cd36* gene knockout.

Blood cell characterization

For non-terminal blood collection, mice were anesthetized with isoflurane and 70 µL of blood collected from the retro-orbital capillary bed using heparinized capillaries and transferred into EDTA-coated tubes (BD Microtainer™ Capillary Blood Collector). Platelet count, size, and basic blood parameters were obtained using an automated cell counter (XN-1000™ Sysmex).

Thiazole Orange analysis

Whole blood (5 µL) was diluted in 500 µL Tyrode's buffer. 50 µL of diluted blood was incubated with 200 ng mL^{-1} of thiazole orange (TO) and an antibody against CD41/61 (Emfret Analytics) was used to identify platelets. TO-positive platelets were identified by flow cytometry (Accuri C6 plus, BD Biosciences).

Platelet Isolation

For terminal bleeds, mice were anaesthetized using 2% isoflurane and blood was collected from the inferior vena cava into EDTA containing tubes. Platelet-rich plasma (PRP) was obtained by centrifugation at 200*g* for 10 minutes (acceleration 9, break 6). After addition of PGI1 (final concentration 560 nM, P5515 Sigma) and Apyrase (final concentration 0.02 U/mL, A6123-500U Sigma), PRP was spun down at 800*g* for 10 minutes (acceleration 9, brake 6). Platelets were washed twice in modified Tyrode's buffer (134 mM NaCl, 2.9 mM KCl, 20 mM HEPES, 1 mM $MgCl_2$, 5 mM Glucose, pH 6.5) containing PGI1 and Apyrase (10 min at 800*g* with acceleration 9 and break 6). After the last wash, the platelet pellet was resuspended in modified Tyrode's buffer.

Platelets were counted on the ProCyte Dx and diluted in PBS to a final concentration of 10,000 platelets/μL. Samples were stored at -80°C prior to lipidomics studies.

Platelet lifespan

Fifty mg of MilliporeSigma™ Calbiochem™ Biotin-NHS, Water-Soluble (Cat: 20-311-8) was injected intravenously into each mouse. At the indicated time points, 50 μL of blood was collected and incubated with 1μL Streptavidin (Alexa Fluor™ 488 Conjugate, Invitrogen, Cat: S11223) and 1 μL PE-conjugated anti-CD41 antibody (BioLegend, Cat:133906) for 10 minutes at room temperature. The percentage of double positive platelets was determined by flow cytometry (Accuri C6 plus, BD Biosciences). Platelet lifespan was determined by measuring the percentage of biotin-labeled platelets over time.

Isolation of murine fetal liver-derived MKs

Fetal liver-derived MKs were cultured from fetal livers as previously described.[41] Briefly, pregnant CD-1 mice at day 13.5 of gestation mice were sacrificed by CO_2 asphyxiation followed by cervical dislocation and fetal livers were extracted. Homogenized fetal liver cells were then cultured in complete media (Dulbecco's Modified Eagle Medium (Sigma), 10% Fetal Bovine Serum, (Sigma) and 1% Penicillin Streptomycin (Gibco)) in the presence of recombinant murine thrombopoietin (50 ng/mL) for 4 days. On day 4, mature MKs were enriched using a bovine serum albumin (BSA) density gradient.

Isolation of murine bone marrow-derived MKs

Mice were sacrificed and long bones and iliac crests were isolated and bone marrow was obtained by centrifugation at 2500*g* for 40s as previously described.[42] HSPCs were separated by lineage depletion using an antibody mixture (Lineage depletion panel, 133307, Biolegend) and magnetic beads (CD4 untouched, 11415D, Invitrogen). For MK maturation, HSPCs were incubated in complete medium containing TPO (50 ng/mL) and recombinant hirudin (100 U/mL, Aniara Diagnostics, RE120A) for 4 days.[43] Differentiated MKs were enriched using a BSA density gradient.

HSPC panel

Mice were sacrificed, long bones and iliac crests isolated, and bone marrow was obtained by centrifugation as described above. Bone marrow cells were filtered using a 70 μm PluriStrainer filter (Pluriselect). Red blood cell lysis was performed according to the manufacturer's instructions (Lysis Buffer, 555899, BD Biosciences). Cells were stained as follows:
For each sample, 1 μL of each antibody (1:100) and 50 μL of BV staining buffer was added. The antibodies used were the following: Pacific Blue™ anti-mouse Lineage Cocktail with Isotype Ctrl (Clones 17A2; RB6-8C5; RA3-6B2; Ter-119; M1/70, (Biolegend, 133305)), APC CD117 (c-Kit) Monoclonal Antibody (clone 2B8, eBioscience™, 17-1171-82), PerCP/Cyanine5.5 anti-mouse Ly-6A/E

(Sca-1) Antibody (clone D7, Biolegend 108123), Brilliant Violet 605™ anti-mouse CD41 Antibody (clone MWReg30, Biolegend133921), APC/Cyanine7 anti-mouse CD48 Antibody (clone HM48-1, Biolegend 103432), BD OptiBuild™ BV786 Rat Anti-Mouse CD34 (clone RAM34, BD Bioscience 742971), PE/Cyanine5 anti-mouse CD150 (SLAM) Antibody (clone TC15-12F12.2, 115912), BD Pharmingen™ PE Rat Anti-Mouse CD13 (clone R3-242, BD Bioscience 558745), PE/Cyanine7 anti-mouse CD105 Antibody (clone MJ7/18, Biolegend 120409).
Unstained samples from both groups, single stained samples, single color beads (1 μL of antibody and 1 drop of UltraComp eBeads Plus Compensation Beads, Invitrogen), and FMO controls were used. Cells were stained for 30 min, followed by 2 consecutive washes with MACS running buffer (Miltenyi). Prior to measuring the sample, DAPI (150 nM) was added, and cells were filtered using a 70 μm PluriStrainer filter. Samples were analyzed using a Spectral Flow Cytometry, Cytek Aurora (Cytekbio). Gating strategies are shown in Extended data Figure 6.

Cell sorting for lipidomics

Bone marrow cells were filtered using a 100 μm filter (Pluriselect). Red blood cell lysis was performed according to the manufacturers' instructions (Lysis Buffer, 555899, BD Biosciences). MEP (Lin-, Sca-1, c-Kit+, CD34-, FcgR-, 10,000 cells) and MK (immature: CD41+, and mature: CD41+/CD42d+ double positive, 10,000 cells) populations were isolated using fluorescence activated cell sorting according to published studies.[44] Samples were sorted using a BD FACS Aria IIu (BD bioscience).

Lipid extraction

Cell samples were lyophilized using either a Savant SpeedVac (Thermo Scientific) or a CoolSafe freeze dryer (ScanVac) prior to extraction and resuspended in 10 µL MilliQ H_2O. Lipids were extracted using a modified single-phase chloroform/methanol extraction method.[45] Briefly, 200 µL chloroform-methanol (2:1) was added to each sample along with an internal standard (ITSD) mixture containing stable-isotope labelled or non-physiological lipids. In tandem, blank control samples and plasma QCs were extracted and dispersed evenly throughout the extraction order to ensure optimal assay performance and to monitor variation that may arise from the extraction. Samples were subsequently mixed with a rotary mixer for 10 mins at 1g, sonicated for 30 mins at room temperature and centrifuged at 11,337*g* for 10 mins to precipitate proteins from the lipid extracts. Supernatant containing the extracted lipids were transferred to a 96 well plate and evaporated using a Savant SpeedVac. Once dried, extracts were reconstituted in H_2O-saturated butanol and methanol with 10 mM ammonium formate and moved to glass vials and stored until mass spectrometry analysis.

Liquid chromatography tandem mass spectrometry (LC-MS/MS)

Lipid extracts were analyzed using an Agilent 6490 triple quadrupole (QqQ) mass spectrometer coupled to an Agilent 1290 high performance liquid chromatography (HPLC) system as previously published[46]. Briefly, we used a ZORBAX eclipse plus C18 column (2.1x100mm 1.8µm, Agilent) with thermostat set to 45°C. The final mass spectrometry analysis on each cell population was

performed in positive mode with dynamic scheduled MRM. Solvents consisted of solvent A (50% H2O, 30% acetonitrile, 20% isopropanol with 10 mM ammonium formate) and solvent B (1% H2O, 9% acetonitrile, 90% isopropanol with 10 mM ammonium formate) and followed a modified 20-minute gradient as shown in **Supplementary Table 1.**

A wash vial comprising of 1:1 butanol:methanol was used after each sample injection. To further improve chromatic peak shape for many anionic/acidic lipid species (notably PS, PA, PIP, S1P), an additional pre-run passivation step was done with phosphoric acid to minimize interaction between the HPLC unit and these lipids. The m/z pairs used for each lipid species can be found in **Supplementary Table 2.**

Lipid nomenclature

The lipid names used follow guidelines set by the LIPIDMAPS consortium.[47] Phospholipids with detailed characteristics i.e., acyl chain composition are annotated as [PC(16:0_20:4)] with PC being the lipid class and (16:0_20:4) representing the acyl chains found on the glycerol backbone, irrespective of sn1 or sn2 position. Lipids without specific structural annotations are named based on their sum acyl chain length and degrees of saturation e.g. PC (36:4). Isomeric lipid species separated chromatographically but incompletely annotated were designated (a), (b) etc., with (a) and (b) representing elution order. Owing to technical limitations, we were unable to assign acyl chains to a specific sn1 or sn2 position for the majority of PL species, only that the acyl chain was present at either the sn1 or sn2 position. In the case of ether-PC and PE, the alkyl or alkenyl chains were always located at the sn1 position and the acyl chain always at the sn2 position. In addition, we were unable to determine acyl chain composition for all PLs and the data shown therefore represents those PLs for which we were able to obtain information on their structural composition. Notably, this represents >90% of total PLs for all cell types.

Analysis of lipids

Individual analyte areas were divided by the area of the corresponding internal standards (ITSDs), and the median of ITSD containing blank samples was subtracted from each analyte (background subtraction). Background subtracted values were multiplied by the concentration of the ITSD and the analyte's respective response factor (Rf). Zeroed background subtraction values (i.e., sample values which were lower than the median blank + ITSD samples) were replaced with 1/10th of the minimum value for the corresponding analyte. Data was ultimately normalized to pmol/µmol of total lipidome where background subtracted data for an individual lipid was divided by the sum of the total lipidome of the sample and multiplied by a factor of 10^6. This allowed us to interrogate the lipid composition of the cellular membrane independently of cell size and protein content. Accurate normalization to protein content was not feasible due to the small rare cell populations and small sample sizes.

tSNE plots were generated in R version 3.6.2 (AN). The data points were initially log10 transformed and unit variance is scaled. The pairwise distances were computed to determine the similarity between the data points followed by the calculation of the probability distribution for each data point. Following data optimization, the data points are plotted creating a visual presentation

of the structure of the high-dimensional data, with similar points appearing close together in the plot. Normalized raw data can be found in supplemental data.

Lipid Enrichment Analysis

Lipid ontology analysis was performed using Lipid Ontology (LION). Analysis was conducted in ranking mode with lipidomic data normalized to mol%. LION-term enrichment was considered significant when FDR q value < 0.05.

RNAseq dataset and Enrichment Analysis

The mRNA seq dataset was previously published by our group.[19] To corroborate if lipid-related genes were differently regulated in non-proplatelet-forming MKs vs proplatelet-forming MKs, the dataset was examined for keywords (e.g lipid, phospholipid, coA, fatty acid, CD36). Selected genes with p value and fold change were plotted using Prisma. Enrichment analysis was done using Reactome.[48]

Flow cytometry on cultured MKs

At day 4 of mauration, MK cultures were centrifuged and washed with autoMACS® Running Buffer (130-091-221, Miltenyi). Cells were stained for 30 min using CD41-FITC (133904, BioLegend) and CD42d-APC (148506, BioLegend) antibodies. Unstained and single cell controls were included. After the incubation, cells were washed twice and analyzed on a FACScalibur (BD Biosciences). The percentage of CD41- and CD41/CD42d-positive cells was analyzed using FlowJo and normalized to the vehicle.

Cytotoxicity assay

The lactate dehydrogenase (LDH) cytotoxicity assay was performed according to the manufacturers' instructions (C20300, ThermoFisher Scientific). Mature FLMKs were treated with indicated dosages of Triacsin C (T4540, Sigma), PF-05175175 (PZ0299, Sigma), and Cerulenin (C2389, Sigma) and incubated overnight in a 96-well-plate and LDH activity in the supernatant was measured. As a positive control, cells were lysed with TritonX-100. MKs treated with vehicle were treated as a negative control (baseline).

Analysis of proplatelet formation using the Incucyte automated microscope

Fetal liver- or bone marrow-derived MKs were isolated by density gradient as described above. MKs were either untreated, supplemented with different fatty acids, or treated with inhibitors (Triacsin C, T4540, Sigma), PF-05175175 (PZ0299, Sigma), Cerulenin (C2389, Sigma), as indicated. For supplementation, MK were treated with palmitic acid (P0500, Sigma) or arachidonic acid (A-122, Sigma) in serum-free media. Proplatelet formation was visualized on the Incucyte

imaging system and quantified using a custom image analysis pipeline or manually by counting the percentage of MKs making proplatelets, using Image J, as described.[49]

Immunostaining of proplatelet-forming MKs

Bone marrow HSPCs were cultured as described above and MKs isolated by density gradient enrichment. MKs were treated with inhibitors or supplemented with different fatty acids as indicated (see below). After treatment, cells were pipetted gently onto the bottom of a μ-side 8-well Ibidi chamber coated with an anti-CD31 antibody (102502, BioLegend) and incubated overnight. The following day, cells were fixed using 4% PFA containing 0.1% Tween20 for 30 min, followed by 3% BSA, and stained for α-tubulin (A488, 322588, ThermoFisher), F-actin (Phalloidin-Atto647N, A22287), and DAPI (Sigma) overnight. Proplatelet formation was visualized using a Zeiss LSM880 confocal microscope (40x objective).

Oxygen Consumption Measurement

MKs were suspended in XF base medium DMEM (Agilent Bioscience) supplemented with 1 mM sodium pyruvate (Agilent Bioscience), 2 mM glutamine (Wisent), and 10 mM glucose (Agilent Bioscience), pH 7.4. A total of 10,000 MKs per well was seeded on XF-96 plates (Agilent/Seahorse Bioscience). Cells were treated with Triacsin C (T4540, Sigma), PF-05175175 (PZ0299, Sigma), or Cerulenin (C2389, Sigma) at the indicated concentrations in complete media for 90 min prior to measurement. Plates were then centrifugated at 300*g* for 2 min at room temperature. We ensured cell homogeneous repartition under a microscope and plates were maintained at 37°C without CO_2 for approximately 60 min prior to loading. Oxygen consumption rates were measured in accordance with manufacturer instructions (Agilent/Seahorse Bioscience). Experiments were replicated in three to five wells and averaged for each experimental condition. A total of 3 measurements of oxygen consumption for each condition were made approximately every 10 min (mix for 3 min, wait for 4 min and measure for 3 min) under basal conditions and after sequential injection of oligomycin (4 μM), FCCP (carbonyl cyanide 4-(trifluoromethoxy) phenylhydrazone, (1 μM) and rotenone/antimycin A (1 μM each). Oligomycin is used as an ATP synthase inhibitor, FCCP as an uncoupling agent of oxidative phosphorylation, rotenone as a complex I inhibitor, and antimycin A as a complex III inhibitor. This allowed us to estimate the contribution of individual parameters for basal respiration, proton leak, maximal respiration, spare respiratory capacity, non-mitochondrial respiration, and ATP production.

Lipid incorporation through click-chemistry

HSPCs were isolated as described above. After lineage depletion, cells were supplemented with fatty acids modified with a ω-terminal alkyne group (Palmitic acid, 13266; Arachidonic Acid, 10538; Cayman Chemical). After 4 days of maturation, click-chemistry was performed using green-fluorescent Alexa Fluor® 488 azide (C10641, ThermoFisher Scientific) according to the manufacturers' instructions. Azides are specifically reactive with terminal alkynes via a copper-

catalyzed click reaction.[50,51] Cells were image using a Zeiss LSM880 confocal microscope (20x and 63x objectives). For analysis, Alexa Fluor® 488 MFI was measured using Image J and normalized to vehicle.

MK ploidy analysis

Bone marrow was isolated from 1 femur by centrifugation at 2500*g* for 40 seconds. Cells were filtered through a 100 µm cell strainer and red blood cells were lysed using ACK buffer (A1049201, Gibco). Cells were washed in PBS, fixed, and permeabilized in 100% ethanol for 30 min on ice. Cells were treated with RNAse A (EN0531, ThermoFisher Scientific) and stained with an anti-CD41-FITC antibody (133904, BioLegend) and propidium iodide (P1304-MP, Sigma Aldrich) for 30 min on ice. Ploidy distribution and percentage of CD41-positive cells were quantified by flow cytometry (BD AccuriC6 Plus).

Cryosectioning and immunofluorescence staining

Mice were sacrificed and femurs isolated and fixed in 4% PFA overnight. Femurs were transferred into 10% sucrose in PBS and a sucrose gradient was performed over 3 days. Femurs were sectioned at 10 µm using a Cryostat CM3050 S (Leica Biosystem), transferred onto slides using a tape-transfer system[52], and rehydrated in PBS for 15 min. Sections were blocked using 5% goat serum and stained using antibodies against CD41 (133902, Biolegend) and laminin (L9393, Sigma) overnight. The following day, sections were incubated with secondary antibodies (goat anti-rat A488 and goat anti-rabbit A647, respectively). After washing in PBS containing 0.1% TritonX 100, DAPI was added for 5 min and the slides were mounted using Fluoroshield (Sigma Aldrich). Image acquisition was performed using a 20x objective (Zeiss LSM880). MK number and area were quantified manually using ImageJ Software (NIH).

Patient recruitment and testing

Patients were consented and recruited to the GAPP study from multiple collaborating Hemophilia Centers across the UK and Ireland as previously described[53] and approved by the UK National Research Ethics Service by the Research Ethics Committee of West Midlands (06/MRE07/36). The study cohort currently consists of >1000 patients with a history of bleeding and suspected of having a platelet disorder of unknown cause. Platelet counts, mean platelet volume (MPV) and other hematological parameters were measured on the Sysmex Whole Blood Analyzer. Whole exome sequencing (WES) was performed in patient genomic DNA as previously reported.[54] For WES filtering of candidate genetic variants was performed to identify rare variants and final sequence variants were confirmed in patients using Sanger sequencing.

Candidate gene panel analysis

Whole exome sequencing analysis was carried out using the bioinformatic pipeline workflow which identified an average of 38,812 variants per individual sample. The bioinformatic pipeline

was used to refine the variants using a series of filtering steps as displayed in Extended data Fig 6. The variants were filtered against a panel of 358 genes known or predicted to be associated with platelet count, function, or lifespan. On average, 222 variants from the gene panel were identified per individual. These variants where then filtered, excluding all synonymous and intronic variants followed by excluding all variants with a MAF of more than 0.01. On average, 16 sequence variants with a MAF of ≤ 0.01 were noted among patients in the panel of 358 platelet related genes. Pathogenicity of the variants was predicted by utilizing the prediction tools (Mutation Taster, PolyPhen-2, SIFT, Provean) and the variants were classified based on the ACMG guidelines. This gave an average of 9 sequence variants per patient. The resulting sequence variants are shown in Extended Data Table 2.

Functional analysis of CD36 mutants and expression

The Q5 Site-Directed Mutagenesis (SDM) Kit (NEB®, USA, #E0554S) was used to introduce the *CD36* heterozygous stop gain variant (c.975T>G; p. Tyr325Ter) into the human *CD36* cDNA wild-type cloned into the mammalian expression pEF-BOS[55] using the following primers:

SDM_CD36 F_Deletion	5'- GTATGTACCAAAAAATATTGCTTC
SDM_CD36 R_Deletion	5'- CTATGATGTACAATTTTTTGAGATAATTTTTTC
SDM_CD36 F_Substitution	5'- GTACATCATAGGGTGTGCTAG
SDM_CD36 R_Substitution	5'- AATTTTTTGAGATAATTTTTTCTGTG

Jurkat T (TIB-152) and HEK293 (CRL-1573) were purchased at American Type Culture Collection (ATCC). The NFAT-luciferase reporter assay was used as previously described.[56] Briefly, Jurkat T cells were electroporated with 20 µg NFAT-luciferase construct and 12.5 µg of either wildtype *CD36* or mutant *CD36* constructs. Twenty-four hours post transfection, cells were harvested and purified, and flow cytometry and western blot analyses were used to assess expression levels.

Statistics and Reproducibility

The results are presented as mean ± standard deviation (SD). Data distributions were analyzed using the Shapiro-Wilk-test and differences between control and mutant mice were statistically analyzed using unpaired, two-tailed Student's t-test, and one- or two-way ANOVA. Tukey, Dunnett or Sidak's post-hoc tests were used for multiple comparisons, as indicated. P-values < 0.05 were considered statistically significant. For representative images, each experiment was repeated three times independently, with equivalent results.

Data Availability

All data supporting the findings in this study are included in the main article and associated files. Source data are provided with this manuscript. All raw lipidomics data can be found at: https://www.ebi.ac.uk/metabolights/MTBLS8042

Code Availability

Instructions and code for the automated pipeline analysis of proplatelet production from megakaryocytes can be found at: https://github.com/broadinstitute/Italiano-MK-Analysis

Acknowledgements

This work is supported by: the National Institutes of Health, National Institute of Diabetes and Digestive and Kidney Diseases (R03DK124746 to KRM, R01DK112778 to JPL) and National Heart, Lung, and Blood Institute (R01HL151494 to KRM, 5T32HL007734 to TH, R35HL161175 to JEI), fellowships from the American Society of Hematology (ASH Restart Award to MNB) and the American Heart Association (23POST1011433 to MNB), a Walter Benjamin Fellowship from the German Research Foundation (DFG; BE 7766/2-1 to ICB), the Boston Children's Hospital Surgical Foundation (TH and MP), the Wellcome Trust (218649/Z/19/Z to AOK), the Saudi Arabia Cultural Bureau in London (IA), the National Health and Medical Research Council of Australia (APP1194329 to AJM and Investigator Grant 2009965 to PJM), the Fonds de Recherche en Santé du Québec and Canadian Institutes of Health Research (EB), and the US Department of Agriculture (USDA) National Institute of Food and Agriculture (to JPL).

We would like to thank Drs. Connie Koo and Mike Tomlinson from the University of Birmingham (Birmingham, UK) for assistance with *in vitro* characterization of the CD36 mutation and Dr Beatrice Nolan (Trinity College Dublin) for referring the patients to the GAPP study. We would also like to thank Dr. Mathieu Laplante (University of Laval, Quebec, CA) and his team for their help with experiments and for being an excellent collaborator. Thank you to Dr. Jessica Cardenas (The University of Texas Health Science Center at Houston) and Dr. Luis Batista (Washington University in St. Louis) for their critical review of the manuscript, excellent edits, and support during the publishing process.

Author Contributions Statement

MNB conceived the study, performed experiments, collected, interpreted, and analyzed data, and wrote the manuscript. GP, ICB and IA performed experiments, collected, and analyzed data. AOK provided intellectual input. EC designed and developed image analysis methodologies. DJG, DF, KG, ZW and IA performed experiments and analyzed data. TH and MP maintained the CD36 knockout mouse colony. JPL performed experiments and analyzed data. NVM recruited and governed the patient's ethics, performed experiments, analyzed data, and helped to draft the manuscript. PJM and TJC analyzed data and prepared figures. NAM performed experiments and analyzed data. PJM and JEI provided intellectual input and key reagents. EB provided intellectual input and interpreted data. AJM helped conceive the lipidomic study, interpret the data, and write the manuscript. KRM conceived and directed the study, analyzed and interpreted data, and wrote the manuscript.

All authors provided input on and reviewed the manuscript.

Competing Interests Statement

JEI has financial interest in and is a founder of StellularBio, a biotechnology company focused on making donor-independent platelet-like cells for regenerative medicine. The interests of JEI are managed by Boston Children's Hospital.

All other authors have no conflicts of interest to declare that are relevant to the content of this article.

Tables

Table 1. Patient details and hematologic parameters. Haematologic parameters of patients II.1 and II.2. M: male, F: female, WBC: white blood cell, RBC: red blood cell, Mono: monocyte, IPF: immature platelet fraction, MPV: mean platelet volume. MPV values were shown in the table as (Large) because platelets with large volume are undetectable by the Sysmex analyser. The Sysmex blood cell analyser showed the hematologic parameter normal ranges which were taken from [57].

Patient	II.1	II.2	Normal range
Age	12-16	12-16	__
Sex	M	F	__
WBC	3.55	5.01	M 3.91 – 10.90 x10^9/L F 4.49 – 12.68
RBC	4.73	3.87	M 4.44 – 5.61 x10^{12}/L F 3.92 – 5.08
Monocytes	0.28	0.32	M 0.29 – 0.95 x10^9/L F 0.25 – 0.84
Platelets	79	87	M 166 – 308 x10^9/L F 173 - 390
IPF	24.4	36.8	M 0.8 – 6.3 % F 0.8 – 6.2
MPV	Large	Large	M 9.3 – 12.1 fL F 9.1 – 11.9

Figure Legends

Figure 1. Megakaryocytes and platelets have a unique lipid profile that is enriched in polyunsaturated fatty acids. (**a**) Murine bone marrow cell populations were isolated by fluorescence-activated cell sorting and platelets by sequential centrifugation. Lipids were extracted and analyzed using 20-min gradient HPLC and mass spectrometry (see methods for details), n=8 for MEP and n=4 for all other cell populations. (**b**) T-distributed stochastic neighbor embedding analysis (tSNE) highlights lipidomic differences between MEPs, immature (CD41+) MKs, mature (CD41/42+) MKs, and platelets. (**c**) LION enrichment analysis showing the top 10 upregulated LION terms. (**d**) Bulk RNA sequencing was performed on MKs immediately preceding and during proplatelet formation[19] and heatmap shows the log2FoldChange of selected genes. (**e**) Reactome enrichment analysis from bulk RNA sequencing on MKs reveals that canonical pathways altered include metabolism of lipids, synthesis of very long-chain fatty acyl-CoAs, and fatty acyl-CoA biosynthesis. Color intensity is directly correlated to the false discovery rate. Total percentage of (**f**) phospholipid classes and (**g**) lipid saturation levels of indicated murine bone marrow cell populations in lipidomics analyses. Percentage of SFAs (**h**) and PUFAs with 6+ double bonds (**i**) in indicated cell populations. MEP, n=8 biologically independent samples; CD41+ MKs, CD41/CD42+ MKs and platelets, n=4 biologically independent samples. One-way ANOVA, Tukey's multiple comparison test. Data are presented as mean +/- SD. Illustrations were done using Biorender®

MK: megakaryocyte; MEP: MK-erythroid progenitor; PA: phosphatidic acid; PC: phosphatidylcholine; PE: phosphatidylethanolamine; PI: phosphatidylinositol; PS: phosphatidylserine; PG: phosphatidylglycerol; SFA: saturated fatty acid; MUFA: monounsaturated fatty acid; PUFA: polyunsaturated fatty acid

Figure 2. Fatty acid incorporation and de novo lipogenesis are necessary for MK differentiation and efficient proplatelet formation. (**a**) Schematic of fatty acid functionalization through long chain acyl-coA synthetase (ACSL). Murine bone marrow HSPCs were cultured with TPO and treated with the ACSL inhibitor Triacsin C (1μM and 3μM). (**b**) Representative images after 4 days of treatment, showing MKs (large cells) and surrounding HSPCs. n=5, scale bar=150 μm (**c**) CD41+ and CD41/CD42d+ cells were quantified using flow cytometry, n=5, one-way ANOVA – Dunnett's test (**d**) Schematic of *de novo* lipogenesis. Murine bone marrow HSPCs were cultured with TPO and treated on day 0 with the acetyl-CoA carboxylase (ACC) and fatty acid synthetase (FASN) inhibitors, (**e**) PF-05175157 (0.3 and 1 μM) n=4, one-way ANOVA – Dunnett's test, and (**f**) Cerulenin (1 and 3 μg/mL) n=6, respectively. Cells were quantified by flow cytometry, one-way ANOVA – Dunnett's test. Data are presented as mean +/- SD (**g**) Mature fetal liver MKs (day 4) were treated with inhibitors at indicated dosages and percentage of MKs making proplatelets and proplatelet area were quantified using the Incucyte high content imaging system. (**h**) Representative phase contrast image showing example quantification of round (red outline) versus proplatelet-making (green outline) MKs (vehicle, left, and Triacsin C, 3 μM, right). (**i**) Representative graph of vehicle (grey) and Triacsin C (1 and 3 μM, dark and light yellow, respectively), n=3, Two-way Anova. Data are presented as mean +/- SEM (connecting bars) (**j**) Representative images of vehicle (left), Triacsin 3μM, (right). b-tubulin (cyan), phalloidin (magenta), DAPI (blue). Scale bar=50 μm (**k**) Representative graph of vehicle (grey) and ACC inhibitor, PF-05175175 (0.1 and 0.3μM, dark and light green, respectively), n=3, Two-way Anova. Data are presented as mean +/- SEM (connecting bars), (**l**) Representative images of vehicle (left), PF-05175175 1μM, (right). b-tubulin (cyan), phalloidin (magenta), DAPI (blue). Scale bar=50 μm.

(**m**) Representative graph of vehicle (grey) and FASN inhibitor, cerulenin (1 and 3 μg/mL, dark and light pink, respectively), n=3, Two-way Anova. Data are presented as mean +/- SEM (connecting bars), (**n**) Representative images of vehicle (left), cerulenin 1μg/mL, (right). b-tubulin (cyan), phalloidin (magenta), DAPI (blue). Scale bar=50 μm. Illustrations were done using Biorender®.

Figure 3. A high saturated fat diet significantly alters MK phenotype and reduces platelet counts. (**a**) Schematic of click-chemistry technique where fatty acids modified with an alkyne are supplemented into murine bone marrow HSPC cultures. After 4 days of culture, the fatty acid with the alkyne that incorporated into mature MKs was functionalized with an azide-linked fluorescent reporter to visualize its uptake into cells. (**b**) Murine bone marrow HSPCs from wildtype mice were incubated with 100μM of modified palmitic acid. After 4 days of maturation, MKs were isolated, and the azide-linked fluorescent reported was added. The incorporation of palmitic acid (PA) was visualized using confocal microscopy. PA-alkyne (cyan); DAPI (blue). Scale bar=5 μm. (**c**) MFI of MKs incubated with 10 and 100 μM PA was calculated using ImageJ. n=3, one-way ANOVA – Dunnett's test (**d**) Murine bone marrow HSPCs from wildtype mice were cultured with TPO and supplemented with 10 and 300 μM palmitic acid. Representative images show MK size. MK area was quantified using ImageJ. n=4, one-way ANOVA – Dunnett's test, scale bar=150 μm. (**e**) To examine proplatelet formation, mature MKs (day 4) were supplemented with palmitic acid (100 mM) or DMEM with 0.1% BSA (vehicle), the percentage of MKs making proplatelets at 24h was quantified using the Incucyte high content imaging system. n=4, unpaired t-test, two-tailed (**f**) Male mice were fed a 60% high fat (D12492, Research Diets Inc) or chow diet (D12450B, Research Diets Inc) for 14 weeks. n=16, unpaired t-test (**g**) Mice were weighed at week 14, n=16 mice per group, unpaired t-test (**h**) LT-HSC, ST-HSC, Pre MKs, and MKP cell populations were quantified at week 14 using flow cytometry, n=4, unpaired t-test (**i**) Representative images of bone marrow showing MKs (CD41, blue) and vasculature (laminin, pink) in femur cryosections. Scale bar=50 μm (**j**) MK area and number were quantified manually from femur cryosections using ImageJ. CHOW n=4 and DIO n=7, biological replicates, unpaired t-test, (**k**) Platelet counts were measured using a Sysmex hematology analyzer. CHOW n=12 and DIO n=16 biological replicates, unpaired t-test, two-tailed. Illustrations were done using Biorender®. All data are presented as mean +/- SD.

Figure 4. Platelet counts can be modified in vivo by altering dietary polyunsaturated fatty acid composition. (**a**) Murine bone marrow HSPCs were incubated with arachidonic acid modified with an alkyne group (3 and 10 μM). After 4 days, MKs were isolated and a fluorescently-conjugated azide was added. Incorporation of arachidonic acid was visualized using confocal microscopy and MFI was calculated using ImageJ. n=3, one-way ANOVA – Dunnett's test. Yellow: AA-alkyne (yellow), DAPI (blue); Scale bar=5 μm. (**b**) Murine bone marrow HSPCs from wildtype mice were cultured with TPO and supplemented with arachidonic acid (3 and 10 μM). On day 4, MK area was quantified using ImageJ. n=6 and n=3, respectively, one-way ANOVA – Dunnett's test (**c**) Mature MKs (day 4) were cultured with arachidonic acid at indicated dosages and the percentage of MKs making proplatelets at 24h was quantified using the Incucyte high content imaging system. n=3, unpaired t-test, two-tailed (**d**) Male mice were fed a 60% high fat diet enriched in polyunsaturated fatty acids (PUFAs) (D22050406i, Research Diets Inc) or chow diet (D12450B, Research Diets Inc) for 12 weeks. n=10 mice per group. Body weight (**e**) and glucose levels (**f**) were measured, n=10, 2-way ANOVA, and unpaired t-test, two-tailed, respectively. Platelet counts were measured at week 4 (**g**) and 12 (**h**) using a Sysmex hematology analyzer. n=10, unpaired t-test, two-tailed. Newly made platelets were analyzed by quantifying (**i**)

percentage and (**j**) absolute platelet numbers positive for thiazole orange by flow cytometry, CHOW n=5 and PUFA n=4 biological replicates, unpaired t-test, two-tailed. (**k**) Representative images showing MKs (CD41, blue) and vasculature (laminin, pink) in femur cryosections at week 12. Scale bar=50 μm (**l**) MK area and number were quantified from femur cryosections using ImageJ, CHOW n=4 and PUFA n=3 biological replicates, unpaired t-test, two-tailed. (**m**) Ploidy analysis of native bone marrow MKs assessed by propidium iodide staining and quantified by flow cytometry. n=5, two-way ANOVA. Illustrations were done using Biorender®. All data are presented as mean +/- SD.

Figure 5. Lack of CD36 in mice reduces cellular fatty acid incorporation and impairs proplatelet formation. Platelets and MKs were characterized in adult male wildtype (WT) and *Cd36*$^{-/-}$ mice. (**a**) Platelet counts, mean platelet volume (MPV), and platelet distribution (PDW) were measured using the Sysmex. WT, n=16 and *Cd36*$^{-/-}$, n=20 biological replicates, unpaired t-test, two-tailed. (**b**) Red blood cell and monocyte counts were measured using Sysmex, unpaired t-test, two-tailed, WT n=16 and *Cd36*$^{-/-}$ n=20 biological replicates(**c-e**) HSCs from WT and *Cd36*$^{-/-}$ mice were cultured with palmitic acid or arachidonic acid modified with an alkyne group at indicated dosages. After 4 days of maturation, MKs were isolated, and click-chemistry performed as described. (**c**) Representative images of MKs from WT and *Cd36*$^{-/-}$ mice. MFI was calculated using ImageJ. Blue: palmitic acid (100 μM). scale bar=5 mm. Incorporation of palmitic acid (**d**) and (**e**) arachidonic acid were visualized using confocal microscopy and MFI was calculated using ImageJ. WT n=3 and *Cd36*$^{-/-}$ n=4 biological replicates, unpaired t-test, two-tailed (**f**) Murine bone marrow HSPCs from WT and *Cd36*$^{-/-}$ mice were cultured with TPO. After 4 days of maturation, the number of mature MKs (CD41/CD42d+ cells) was measured using flow cytometry, WT n=3 and *Cd36*$^{-/-}$ n=4 biological replicates, unpaired t-test, two-tailed. (**g**) MK number and area were quantified from femur cryosections using ImageJ. WT n=3 and *Cd36*$^{-/-}$ n=4 biological replicates, unpaired t-test. Representative images show MKs (CD41, blue) and vasculature (laminin, pink). Scale bar=50 μm (**h**) Ploidy analysis of cultured bone marrow MKs assessed by propidium iodide staining and flow cytometry. Percentage of CD41+ cells with different levels of ploidy is shown. n=4, two-way ANOVA. (**i-j**) Proplatelet formation was quantified from mature MKs (day 4) from WT and *Cd36*$^{-/-}$ mice in the presence of hirudin. (**i**) Representative graph of proplatelet area from n=4. Data are presented as mean +/- SEM (connecting bars) (**j**) and proplatelet percentage at 24h, were quantified using the Incucyte high content imaging system. n= 6, unpaired t-test, two-tailed. All data are presented as mean +/- SD.

Figure 6. Megakaryocytes and platelet counts in *Cd36*$^{-/-}$ mice are not affected by high fat diets enriched in fatty acids. Adult male WT and *Cd36*$^{-/-}$ mice were fed chow or high fat diets enriched in saturated or polyunsaturated fatty acids as in Figures 3 and 4, respectively, for 13 weeks. (**a-b**) At week 8, (**a**) platelet counts and (**b**) mean platelet volume (MPV) were measured using Sysmex hematology analyzer and (**c**) newly made platelets were analyzed by quantifying percentage and absolute platelet numbers positive for thiazole orange by flow cytometry. n=3 (CHOW), n=4 (DIO) and n=3 (PUFA) mice per group, One-way Anova test, Dunnett's multiple comparisons test. At week 13, (**d**) platelet counts, (**e**) MPV and (**f**) newly made platelets were measured as above. (**g**) Representative images showing MKs (CD41, blue) and vasculature (laminin, pink) in femur cryosections at week 13 in indicated treatment groups. Scale bar=50 μm. (**h**) MK area and (**i**) number were quantified from femur cryosections using ImageJ, n=3 mice per group. One-way Anova test, Dunnett's multiple comparisons test. All data are presented as mean +/- SD.

Figure 7. Identification of a *CD36* loss-of-function variant (p.Tyr325Ter) in patients with thrombocytopenia. (**a**) Family pedigree including affected mother (I:2) and patients II.1 and II.2. highlighted in solid black. Asterisks (*) indicate patients whose whole exomes were sequenced. (**b**) Patient's details and hematological parameters. Hematological parameters of patients II.1 and II.2. MPV values are shown in the table as 'Large' because platelets with large volume are undetectable by Sysmex analyzer. (**c**) The nonsense variant c.975T>G; p. Tyr325Ter results in the substitution of tyrosine residue at position 325 to a stop codon which is predicted to truncate the full length of 472 amino acids. (**d**) Mutation details (**e**) Western blot of protein lysate from patient platelets showing truncation of CD36 protein and GAPDH loading control (**f**) Conservation of tyrosine 325 residue across multiple species. The location of the tyrosine residue is shown by the highlighted green box. (**g**) Modelled structure of the CD36 ectodomain using homology modeling.[22] The structure shows the result of the CD36 nonsense variant on the structure of the WT CD36 protein (left) and mutant CD36 (right) because of the truncation. (**h**) Schematic of the CD36 protein structure. CD36 has two short cytoplasmic domains representing the C-terminal and N-terminals, two transmembrane domains and two large extracellular domains. The extracellular domain contains three disulfide bonds, binding sites of interaction with thrombospondin type I repeat (TSR), plasmodium falciparum, oxLDL, sites of acetylation (palmitoylation), phosphorylation, glycosylation, and the position of the nonsense variant found in patients II.1 and II.2.[56,57] (**i**) Protein expression of transfected CD36-wild type and CD36 mutants. C: pEF6 empty vector; WT: pEF6/CD36 wild type; Del: pEF6/CD36 deleted mutant; Sub: pEF6/CD36 substitution mutant. SDS-PAGE immunoblot expression analysis of samples probed with anti-CD36 and anti-GAPDH antibodies. Expected sizes of the samples are indicated on the right. (**j**) NFAT-luciferase activity measuring activation of CD36 after normalization of the stimulated and unstimulated conditions. Only WT CD36 shows luciferase activity over background. n=3 biological replicates, One-way Anova test with Dunnett's test. Data are presented as mean +/- SD.

M: male, F: female, WBC: white blood cell, RBC: red blood cell, Mono: monocyte, IPF: immature platelet fraction, MPV: mean platelet volume. WT: wildtype, Del: deletion, Sub: substitution

REFERENCES

1 van Meer, G., Voelker, D. R. & Feigenson, G. W. Membrane lipids: where they are and how they behave. *Nat Rev Mol Cell Biol* **9**, 112-124, doi:10.1038/nrm2330 (2008).

2 Murphy, A. J. *et al.* ApoE regulates hematopoietic stem cell proliferation, monocytosis, and monocyte accumulation in atherosclerotic lesions in mice. *J Clin Invest* **121**, 4138-4149, doi:10.1172/JCI57559 (2011).

3 Bansal, P. *et al.* Current Updates on Role of Lipids in Hematopoiesis. *Infect Disord Drug Targets* **18**, 192-198, doi:10.2174/1871526518666180405155015 (2018).

4 Lee, M. K. S., Al-Sharea, A., Dragoljevic, D. & Murphy, A. J. Hand of FATe: lipid metabolism in hematopoietic stem cells. *Curr Opin Lipidol* **29**, 240-245, doi:10.1097/MOL.0000000000000500 (2018).

5 Pernes, G., Flynn, M. C., Lancaster, G. I. & Murphy, A. J. Fat for fuel: lipid metabolism in haematopoiesis. *Clin Transl Immunology* **8**, e1098, doi:10.1002/cti2.1098 (2019).

6 Collins, J. M. *et al.* De novo lipogenesis in the differentiating human adipocyte can provide all fatty acids necessary for maturation. *J Lipid Res* **52**, 1683-1692, doi:10.1194/jlr.M012195 (2011).

7 Noetzli, L. J., French, S. L. & Machlus, K. R. New Insights Into the Differentiation of Megakaryocytes From Hematopoietic Progenitors. *Arterioscler Thromb Vasc Biol* **39**, 1288-1300, doi:10.1161/ATVBAHA.119.312129 (2019).

8 Machlus, K. R. & Italiano, J. E. The incredible journey: From megakaryocyte development to platelet formation. *J Cell Biol* **201**, 785-796, doi:10.1083/jcb.201304054 (2013).

9 Pietras, E. M. *et al.* Functionally Distinct Subsets of Lineage-Biased Multipotent Progenitors Control Blood Production in Normal and Regenerative Conditions. *Cell stem cell* **17**, 35-46, doi:10.1016/j.stem.2015.05.003 (2015).

10 Eckly, A. *et al.* Biogenesis of the demarcation membrane system (DMS) in megakaryocytes. *Blood* **123**, 921-930, doi:10.1182/blood-2013-03-492330 (2014).

11 Whitaker, B., Rajbhandary, S., Kleinman, S., Harris, A. & Kamani, N. Trends in United States blood collection and transfusion: results from the 2013 AABB Blood Collection, Utilization, and Patient Blood Management Survey. *Transfusion* **56**, 2173-2183, doi:10.1111/trf.13676 (2016).

12 Provan, D. *et al.* Updated international consensus report on the investigation and management of primary immune thrombocytopenia. *Blood Adv* **3**, 3780-3817, doi:10.1182/bloodadvances.2019000812 (2019).

13 Ghanima, W. *et al.* Bone marrow fibrosis in 66 patients with immune thrombocytopenia treated with thrombopoietin-receptor agonists: a single-center, long-term follow-up. *Haematologica* **99**, 937-944, doi:10.3324/haematol.2013.098921 (2014).

14 Mitchell, W. B. & Bussel, J. B. Thrombopoietin receptor agonists: a critical review. *Semin Hematol* **52**, 46-52, doi:10.1053/j.seminhematol.2014.11.001 (2015).

15 Prica, A., Sholzberg, M. & Buckstein, R. Safety and efficacy of thrombopoietin-receptor agonists in myelodysplastic syndromes: a systematic review and meta-analysis of randomized controlled trials. *Br J Haematol* **167**, 626-638, doi:10.1111/bjh.13088 (2014).

16 Manni, M. M. *et al.* Acyl chain asymmetry and polyunsaturation of brain phospholipids facilitate membrane vesiculation without leakage. *Elife* **7**, doi:10.7554/eLife.34394 (2018).
17 Valet, C. *et al.* Adipocyte Fatty Acid Transfer Supports Megakaryocyte Maturation. *Cell Rep* **32**, 107875, doi:10.1016/j.celrep.2020.107875 (2020).
18 Kelly, K. L. *et al.* De novo lipogenesis is essential for platelet production in humans. *Nat Metab* **2**, 1163-1178, doi:10.1038/s42255-020-00272-9 (2020).
19 Machlus, K. R. *et al.* Synthesis and dephosphorylation of MARCKS in the late stages of megakaryocyte maturation drive proplatelet formation. *Blood* **127**, 1468-1480, doi:10.1182/blood-2015-08-663146 (2016).
20 Febbraio, M. *et al.* A null mutation in murine CD36 reveals an important role in fatty acid and lipoprotein metabolism. *J Biol Chem* **274**, 19055-19062, doi:10.1074/jbc.274.27.19055 (1999).
21 Aitman, T. J. *et al.* Malaria susceptibility and CD36 mutation. *Nature* **405**, 1015-1016, doi:10.1038/35016636 (2000).
22 Hsieh, F. L. *et al.* The structural basis for CD36 binding by the malaria parasite. *Nat Commun* **7**, 12837, doi:10.1038/ncomms12837 (2016).
23 Escribá, P. V. *et al.* Membrane lipid therapy: Modulation of the cell membrane composition and structure as a molecular base for drug discovery and new disease treatment. *Prog Lipid Res* **59**, 38-53, doi:10.1016/j.plipres.2015.04.003 (2015).
24 Doi, O., Doi, F., Schroeder, F., Alberts, A. W. & Vagelos, P. R. Manipulation of fatty acid composition of membrane phospholipid and its effects on cell growth in mouse LM cells. *Biochim Biophys Acta* **509**, 239-250, doi:10.1016/0005-2736(78)90044-5 (1978).
25 Pinot, M. *et al.* Lipid cell biology. Polyunsaturated phospholipids facilitate membrane deformation and fission by endocytic proteins. *Science* **345**, 693-697, doi:10.1126/science.1255288 (2014).
26 Hales, C. M., Carroll, M. D., Fryar, C. D. & Ogden, C. L. Prevalence of Obesity and Severe Obesity Among Adults: United States, 2017-2018. *NCHS Data Brief*, 1-8 (2020).
27 Yin, R., Wang, X., Li, K., Yu, K. & Yang, L. Lipidomic profiling reveals distinct differences in plasma lipid composition in overweight or obese adolescent students. *BMC Endocr Disord* **21**, 201, doi:10.1186/s12902-021-00859-7 (2021).
28 Vilahur, G., Ben-Aicha, S. & Badimon, L. New insights into the role of adipose tissue in thrombosis. *Cardiovasc Res* **113**, 1046-1054, doi:10.1093/cvr/cvx086 (2017).
29 Badimon, L., Hernández Vera, R., Padró, T. & Vilahur, G. Antithrombotic therapy in obesity. *Thromb Haemost* **110**, 681-688, doi:10.1160/th12-12-0928 (2013).
30 Barale, C. & Russo, I. Influence of Cardiometabolic Risk Factors on Platelet Function. *Int J Mol Sci* **21**, doi:10.3390/ijms21020623 (2020).
31 Haas, S. *et al.* Inflammation-Induced Emergency Megakaryopoiesis Driven by Hematopoietic Stem Cell-like Megakaryocyte Progenitors. *Cell Stem Cell* **17**, 422-434, doi:10.1016/j.stem.2015.07.007 (2015).
32 Couldwell, G. & Machlus, K. R. Modulation of megakaryopoiesis and platelet production during inflammation. *Thromb Res* **179**, 114-120, doi:10.1016/j.thromres.2019.05.008 (2019).

33 Blüher, M. Metabolically Healthy Obesity. *Endocrine Reviews* **41**, doi:10.1210/endrev/bnaa004 (2020).
34 Iacobini, C., Pugliese, G., Blasetti Fantauzzi, C., Federici, M. & Menini, S. Metabolically healthy versus metabolically unhealthy obesity. *Metabolism* **92**, 51-60, doi:10.1016/j.metabol.2018.11.009 (2019).
35 Xu, S., Jay, A., Brunaldi, K., Huang, N. & Hamilton, J. A. CD36 enhances fatty acid uptake by increasing the rate of intracellular esterification but not transport across the plasma membrane. *Biochemistry* **52**, 7254-7261, doi:10.1021/bi400914c (2013).
36 Podrez, E. A. *et al.* Platelet CD36 links hyperlipidemia, oxidant stress and a prothrombotic phenotype. *Nat Med* **13**, 1086-1095, doi:10.1038/nm1626 (2007).
37 Meng, O. *et al.* Loss of Cd36 Expression Has Limited Impact on Mouse Normal Hematopoiesis. *Blood* **140**, 11395-11396, doi:10.1182/blood-2022-171125 (2022).
38 Xu, X., Zheng, X. & Zhu, F. CD36 gene variants and their clinical relevance: a narrative review. *Annals of Blood* **6** (2021).
39 Tomiyama, Y. *et al.* Identification of the platelet-specific alloantigen, Naka, on platelet membrane glycoprotein IV. *Blood* **75**, 684-687 (1990).
40 Strassheim, D. *et al.* Metabolite G-Protein Coupled Receptors in Cardio-Metabolic Diseases. *Cells* **10**, doi:10.3390/cells10123347 (2021).
41 Vijey, P., Posorske, B. & Machlus, K. R. In vitro culture of murine megakaryocytes from fetal liver-derived hematopoietic stem cells. *Platelets* **29**, 583-588, doi:10.1080/09537104.2018.1492107 (2018).
42 Heib, T., Gross, C., Muller, M. L., Stegner, D. & Pleines, I. Isolation of murine bone marrow by centrifugation or flushing for the analysis of hematopoietic cells - a comparative study. *Platelets* **32**, 601-607, doi:10.1080/09537104.2020.1797323 (2021).
43 Strassel, C. *et al.* Hirudin and heparin enable efficient megakaryocyte differentiation of mouse bone marrow progenitors. *Exp Cell Res* **318**, 25-32, doi:10.1016/j.yexcr.2011.10.003 (2012).
44 Huynh, K. *et al.* Lipidomic Profiling of Murine Macrophages Treated with Fatty Acids of Varying Chain Length and Saturation Status. *Metabolites* **8**, doi:10.3390/metabo8020029 (2018).
45 Weir, J. M. *et al.* Plasma lipid profiling in a large population-based cohort. *J Lipid Res* **54**, 2898-2908, doi:10.1194/jlr.P035808 (2013).
46 Huynh, K. *et al.* High-Throughput Plasma Lipidomics: Detailed Mapping of the Associations with Cardiometabolic Risk Factors. *Cell Chem Biol* **26**, 71-84.e74, doi:10.1016/j.chembiol.2018.10.008 (2019).
47 Liebisch, G. *et al.* Update on LIPID MAPS classification, nomenclature, and shorthand notation for MS-derived lipid structures. *J Lipid Res* **61**, 1539-1555, doi:10.1194/jlr.S120001025 (2020).
48 Gillespie, M. *et al.* The reactome pathway knowledgebase 2022. *Nucleic Acids Research* **50**, D687-D692, doi:10.1093/nar/gkab1028 (2021).
49 French, S. L. *et al.* High-content, label-free analysis of proplatelet production from megakaryocytes. *J Thromb Haemost* **18**, 2701-2711, doi:10.1111/jth.15012 (2020).

50 Lutz, J. F. & Zarafshani, Z. Efficient construction of therapeutics, bioconjugates, biomaterials and bioactive surfaces using azide-alkyne "click" chemistry. *Adv Drug Deliv Rev* **60**, 958-970, doi:10.1016/j.addr.2008.02.004 (2008).
51 Hein, C. D., Liu, X. M. & Wang, D. Click chemistry, a powerful tool for pharmaceutical sciences. *Pharm Res* **25**, 2216-2230, doi:10.1007/s11095-008-9616-1 (2008).
52 Kawamoto, T. Use of a new adhesive film for the preparation of multi-purpose fresh-frozen sections from hard tissues, whole-animals, insects and plants. *Arch Histol Cytol* **66**, 123-143, doi:10.1679/aohc.66.123 (2003).
53 Watson, S. P., Lowe, G. C., Lordkipanidzé, M. & Morgan, N. V. Genotyping and phenotyping of platelet function disorders. *J Thromb Haemost* **11 Suppl 1**, 351-363, doi:10.1111/jth.12199 (2013).
54 Johnson, B. *et al.* Whole exome sequencing identifies genetic variants in inherited thrombocytopenia with secondary qualitative function defects. *Haematologica* **101**, 1170-1179, doi:10.3324/haematol.2016.146316 (2016).
55 Thorne, R. F. *et al.* The Integrins α3β1 and α6β1 Physically and Functionally Associate with CD36 in Human Melanoma Cells REQUIREMENT FOR THE EXTRACELLULAR DOMAIN OF CD36. *Journal of Biological Chemistry* **275**, 35264-35275 (2000).
56 Tomlinson, M. *et al.* Collagen promotes sustained glycoprotein VI signaling in platelets and cell lines. *Journal of Thrombosis and Haemostasis* **5**, 2274-2283 (2007).
57 Pekelharing, J. *et al.* Haematology reference intervals for established and novel parameters in healthy adults. *Sysmex Journal International* **20**, 1-9 (2010).

Figure 1

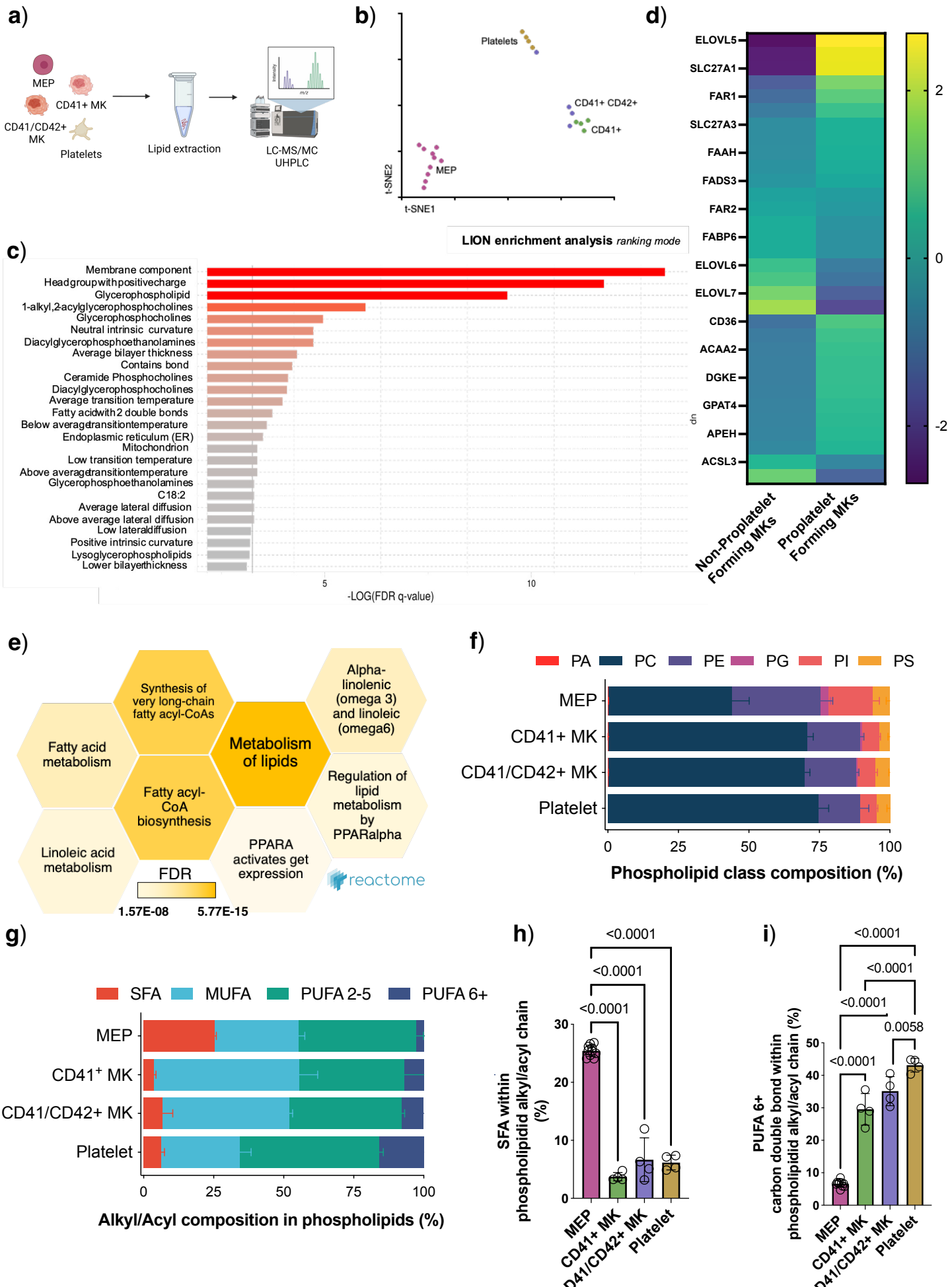
a)
MEP
CD41+ MK
CD41/CD42+ MK
Platelets
Lipid extraction
LC-MS/MC UHPLC
b)
Platelets
CD41+ CD42+
CD41+
MEP
t-SNE2
t-SNE1
d)
ELOVL5
SLC27A1
FAR1
SLC27A3
FAAH
FADS3
FAR2
FABP6
ELOVL6
ELOVL7
CD36
ACAA2
DGKE
GPAT4
APEH
ACSL3
dn
2
0
-2
Non-Proplatelet Forming MKs
Proplatelet Forming MKs
c)
LION enrichment analysis ranking mode
Membrane component
Headgroupwithpositivecharge
Glycerophospholipid
1-alkyl,2-acylglycerophosphocholines
Glycerophosphocholines
Neutral intrinsic curvature
Diacylglycerophosphoethanolamines
Average bilayer thickness
Contains bond
Ceramide Phosphocholines
Diacylglycerophosphocholines
Average transition temperature
Fatty acidwith2 double bonds
Below averagetransitiontemperature
Endoplasmic reticulum (ER)
Mitochondrion
Low transition temperature
Above averagetransitiontemperature
Glycerophosphoethanolamines
C18:2
Average lateral diffusion
Above average lateral diffusion
Low lateraldiffusion
Positive intrinsic curvature
Lysoglycerophospholipids
Lower bilayerthickness
5
10
-LOG(FDR q-value)
e)
Synthesis of very long-chain fatty acyl-CoAs
Alpha-linolenic (omega 3) and linoleic (omega6)
Fatty acid metabolism
Metabolism of lipids
Regulation of lipid metabolism by PPARalpha
Fatty acyl-CoA biosynthesis
Linoleic acid metabolism
PPARA activates get expression
FDR
1.57E-08
5.77E-15
reactome
f)
PA
PC
PE
PG
PI
PS
MEP
CD41+ MK
CD41/CD42+ MK
Platelet
0
25
50
75
100
Phospholipid class composition (%)
g)
SFA
MUFA
PUFA 2-5
PUFA 6+
MEP
CD41+ MK
CD41/CD42+ MK
Platelet
0
25
50
75
100
Alkyl/Acyl composition in phospholipids (%)
h)
<0.0001
<0.0001
<0.0001
SFA within phospholipidid alkyl/acyl chain (%)
30
20
10
0
MEP
CD41+ MK
CD41/CD42+ MK
Platelet
i)
<0.0001
<0.0001
<0.0001
0.0058
<0.0001
PUFA 6+ carbon double bond within phospholipidid alkyl/acyl chain (%)
50
40
30
20
10
0
MEP
CD41+ MK
CD41/CD42+ MK
Platelet

Figure 2

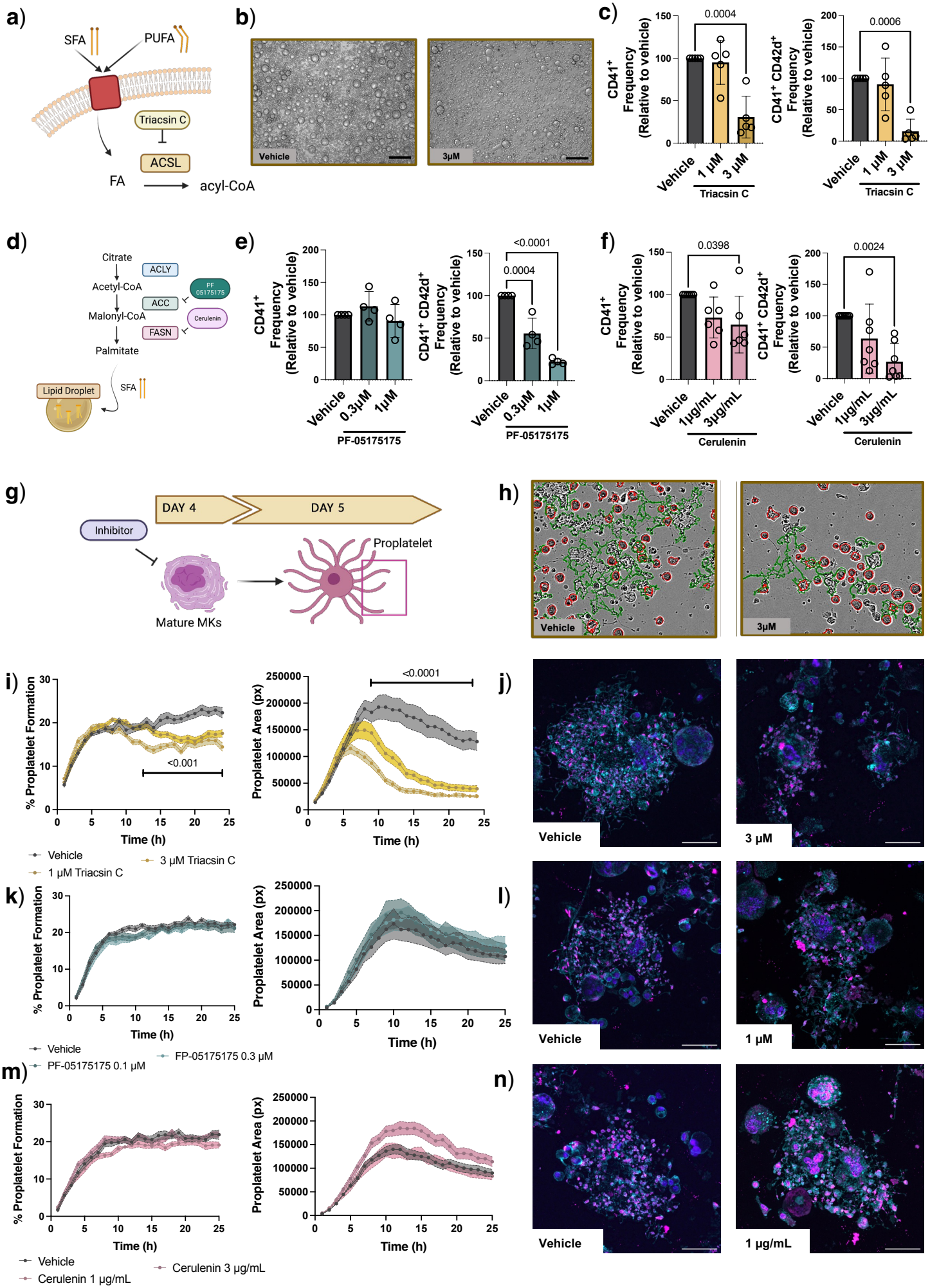
a)
SFA
PUFA
Triacsin C
ACSL
FA
acyl-CoA
b)
Vehicle
3μM
c)
CD41+ Frequency (Relative to vehicle)
0.0004
CD41+ CD42d+ Frequency (Relative to vehicle)
0.0006
Vehicle
1 μM
3 μM
Triacsin C
d)
Citrate
ACLY
Acetyl-CoA
PF 05175175
ACC
Malonyl-CoA
Cerulenin
FASN
Palmitate
Lipid Droplet
SFA
e)
CD41+ Frequency (Relative to vehicle)
CD41+ CD42d+ Frequency (Relative to vehicle)
<0.0001
0.0004
Vehicle
0.3μM
1μM
PF-05175175
f)
0.0398
0.0024
Vehicle
1μg/mL
3μg/mL
Cerulenin
g)
DAY 4
DAY 5
Inhibitor
Proplatelet
Mature MKs
h)
Vehicle
3μM
i)
% Proplatelet Formation
<0.001
Time (h)
Proplatelet Area (px)
<0.0001
Vehicle
1 μM Triacsin C
3 μM Triacsin C
j)
Vehicle
3 μM
k)
% Proplatelet Formation
Time (h)
Proplatelet Area (px)
Vehicle
PF-05175175 0.1 μM
FP-05175175 0.3 μM
l)
Vehicle
1 μM
m)
% Proplatelet Formation
Time (h)
Proplatelet Area (px)
Vehicle
Cerulenin 1 μg/mL
Cerulenin 3 μg/mL
n)
Vehicle
1 μg/mL

Figure 3

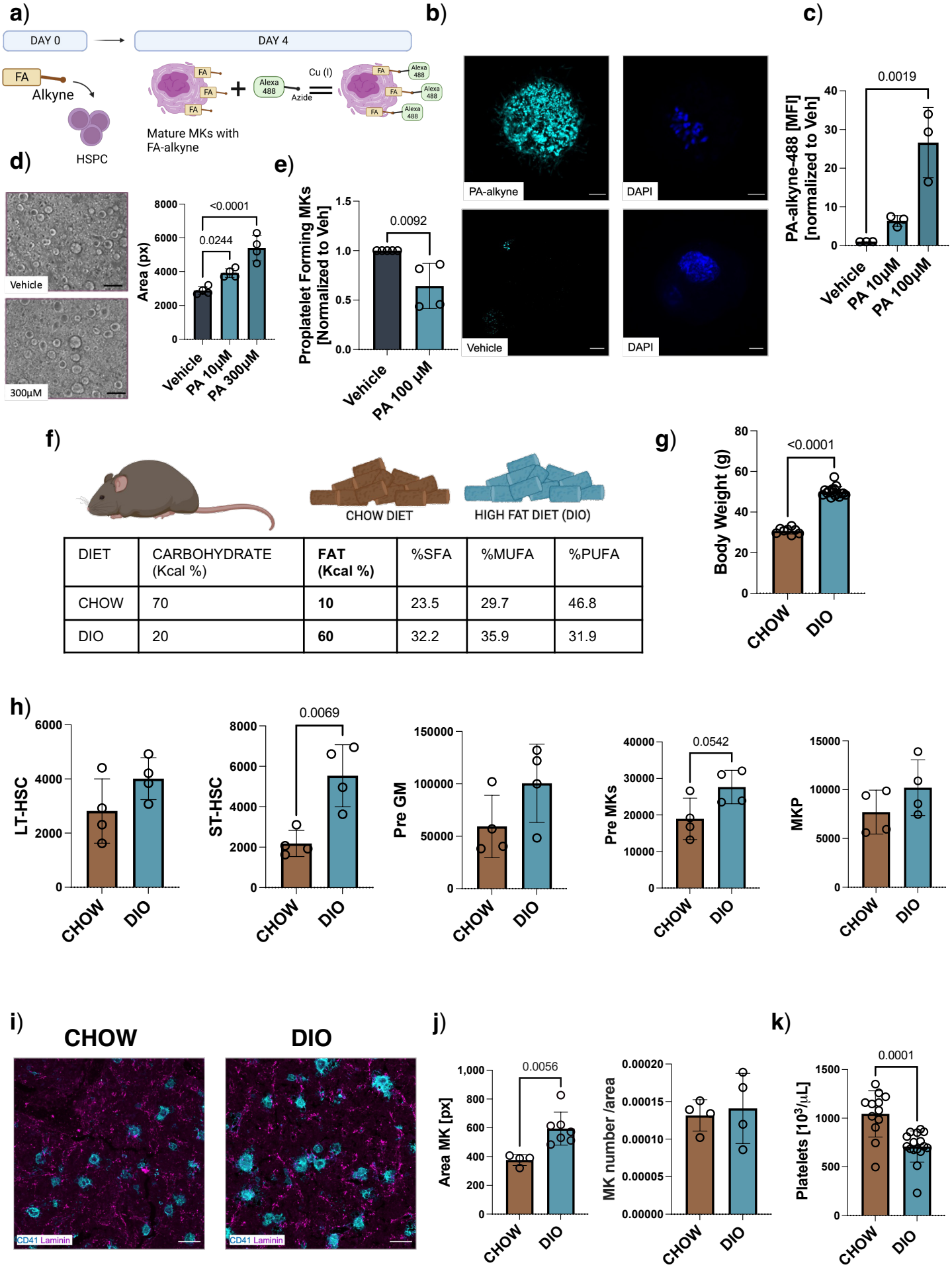

DIET	CARBOHYDRATE (Kcal %)	**FAT (Kcal %)**	%SFA	%MUFA	%PUFA
CHOW	70	**10**	23.5	29.7	46.8
DIO	20	**60**	32.2	35.9	31.9

Figure 4

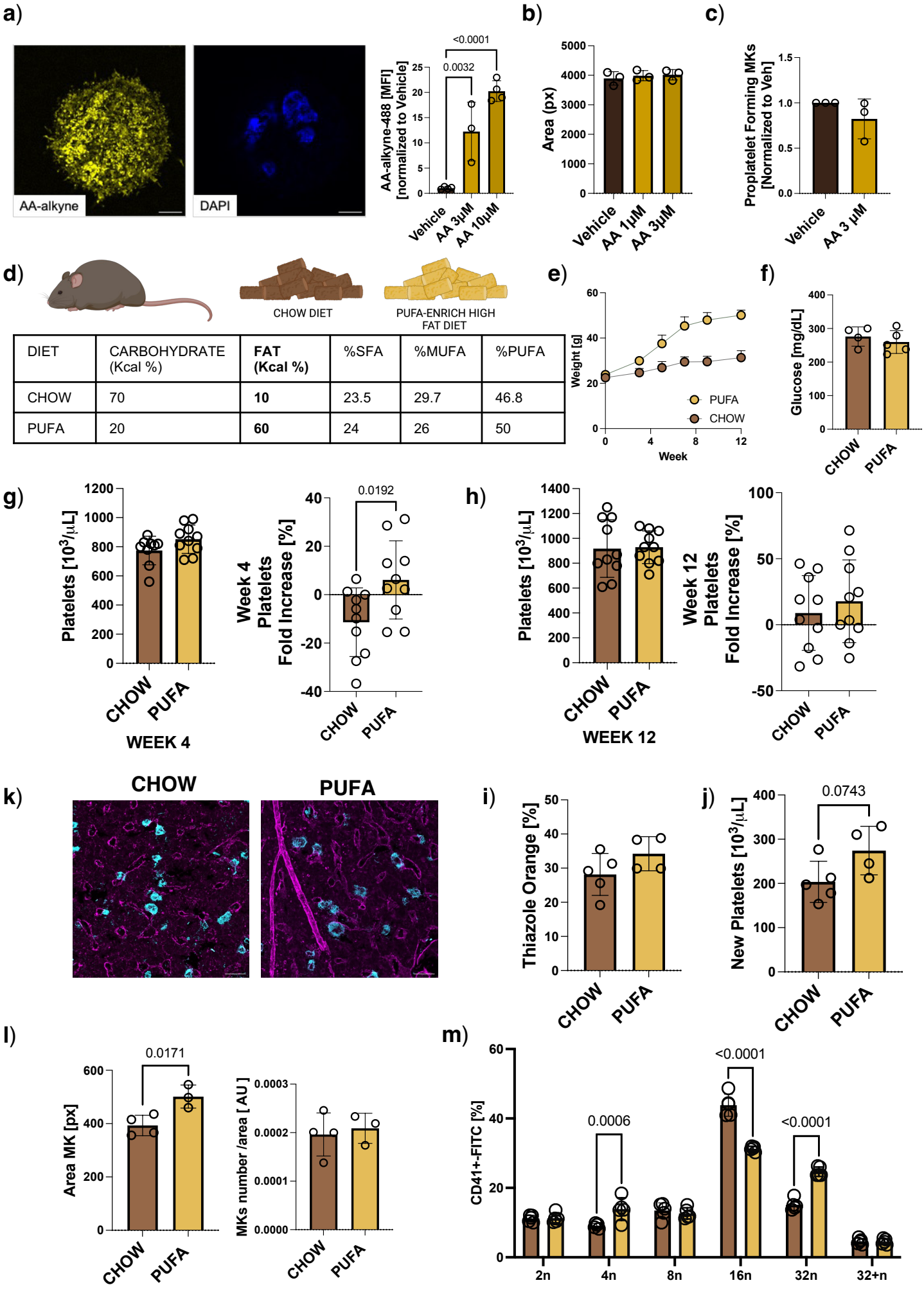

DIET	CARBOHYDRATE (Kcal %)	**FAT (Kcal %)**	%SFA	%MUFA	%PUFA
CHOW	70	**10**	23.5	29.7	46.8
PUFA	20	**60**	24	26	50

Figure 5

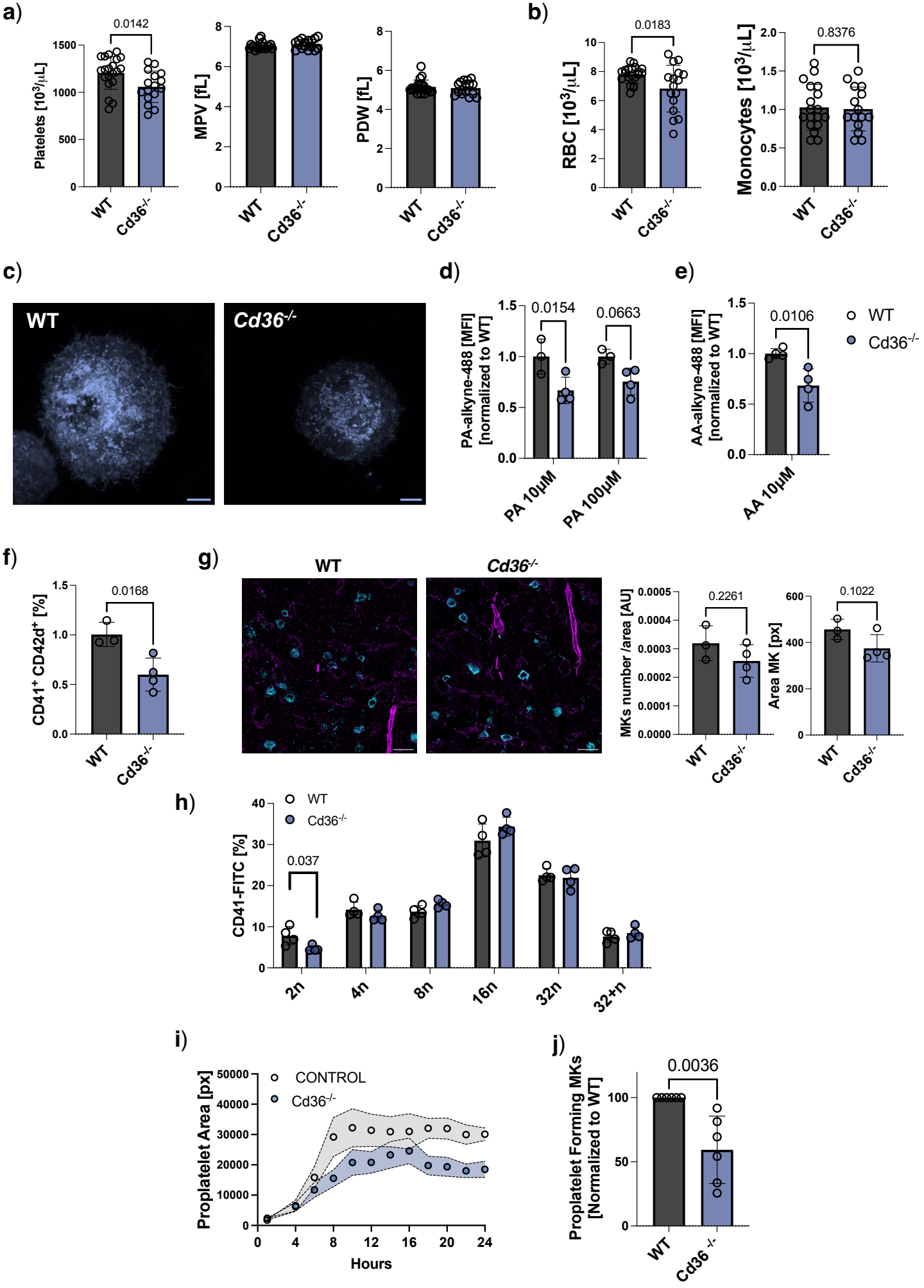
a)
Platelets [10³/μL]
0.0142
MPV [fL]
PDW [fL]
WT
Cd36-/-
b)
RBC [10³/μL]
0.0183
Monocytes [10³/μL]
0.8376
c)
WT
Cd36-/-
d)
PA-alkyne-488 [MFI] [normalized to WT]
0.0154
0.0663
PA 10μM
PA 100μM
e)
AA-alkyne-488 [MFI] [normalized to WT]
0.0106
AA 10μM
WT
Cd36-/-
f)
CD41+ CD42d+ [%]
0.0168
g)
WT
Cd36-/-
MKs number /area [AU]
0.2261
Area MK [px]
0.1022
h)
CD41-FITC [%]
WT
Cd36-/-
0.037
2n
4n
8n
16n
32n
32+n
i)
Proplatelet Area [px]
CONTROL
Cd36-/-
Hours
j)
Proplatelet Forming MKs [Normalized to WT]
0.0036
WT
Cd36-/-

Figure 6

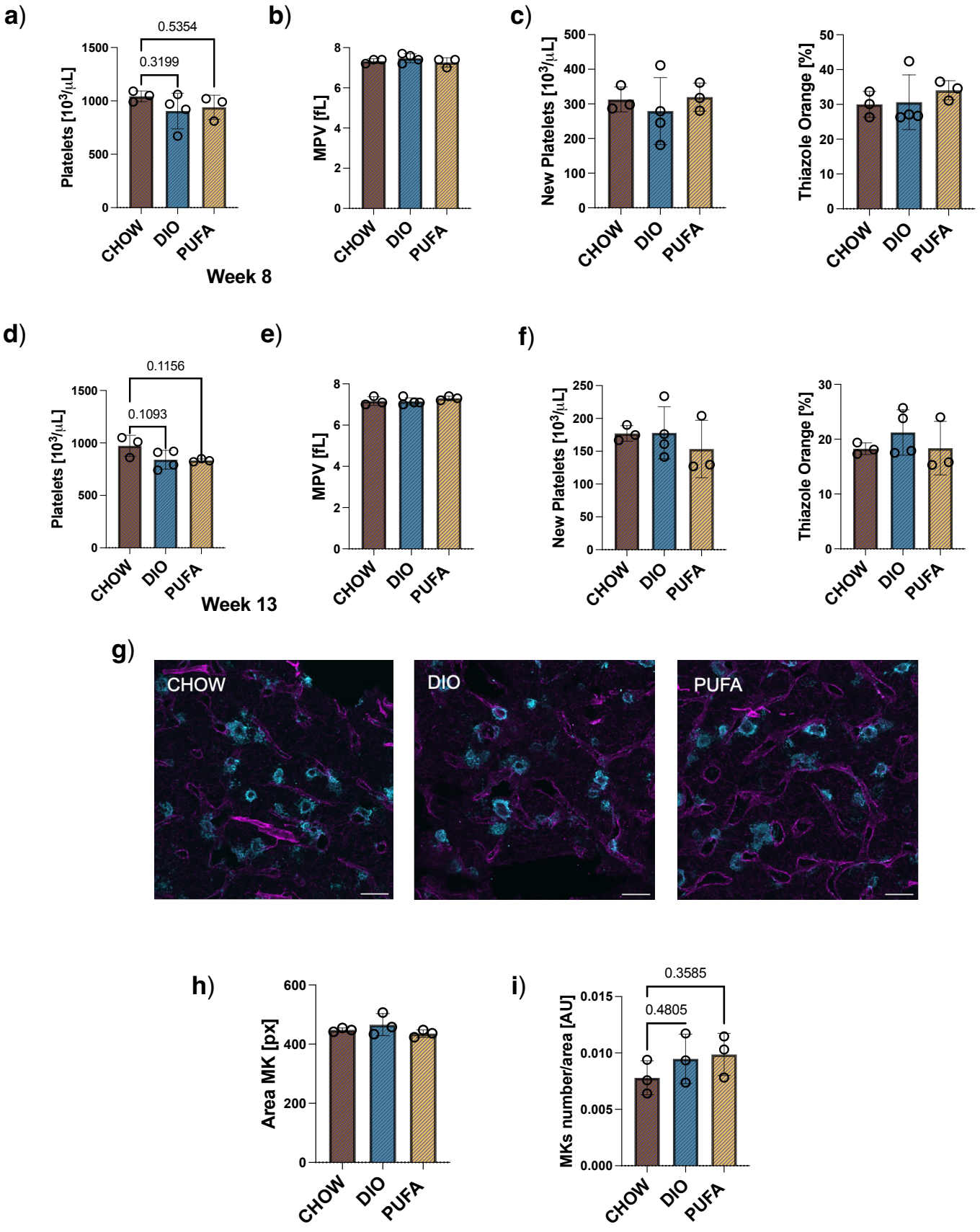
a)
0.5354
0.3199
Platelets [10³/μL]
1500
1000
500
0
CHOW
DIO
PUFA
Week 8
b)
MPV [fL]
8
6
4
2
0
c)
New Platelets [10³/μL]
500
400
300
200
100
0
Thiazole Orange [%]
50
40
30
20
10
d)
0.1156
0.1093
Week 13
e)
f)
250
200
150
100
50
g)
CHOW
DIO
PUFA
h)
Area MK [px]
600
400
200
i)
0.3585
0.4805
MKs number/area [AU]
0.015
0.010
0.005
0.000

Figure 7

a)

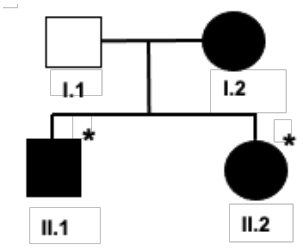

b)

Patient	II.1	II.2
Age	12-16	12-16
Sex	M	F
Platelet Count (x10^9/L)	79	87
IPF	24.4	36.8
MPV	Large	Large

c)

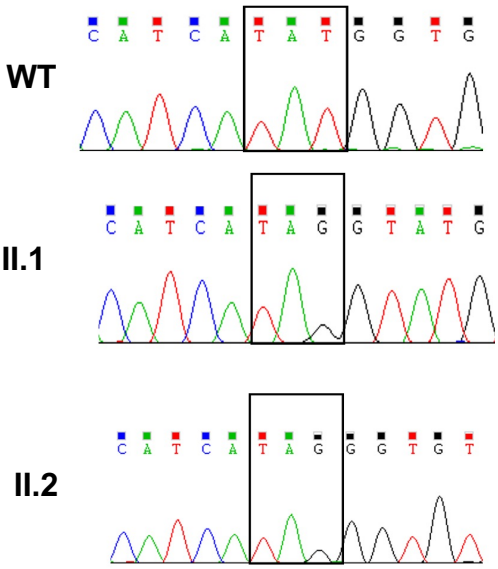

d)

Patient	Gene	Genomic variation	Protein effect	Variation type	Prevalence	Mutation taster	ACMG criteria	Classification
II.1	*CD36*	c.975T>G	p. Tyr325Ter	stop gained	0.007914	Polymorphism	PVS1,PS3,PP1, PP5	Pathogenic
II.2	*CD36*	c.975T>G	p. Tyr325Ter	stop gained	0.007914	Polymorphism	PVS1,PS3,PP1, PP5	Pathogenic

e)

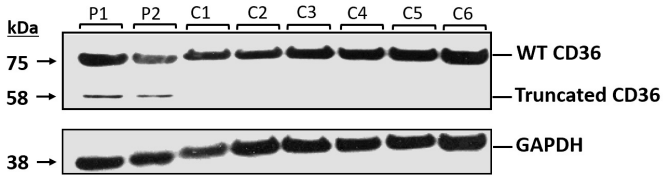

f)

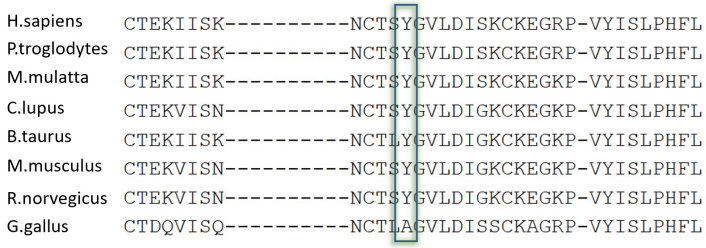

g) CD36 WT

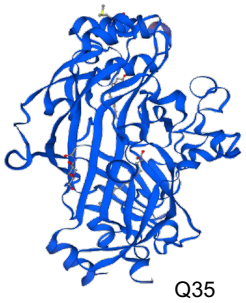

CD36 Y325X

h)

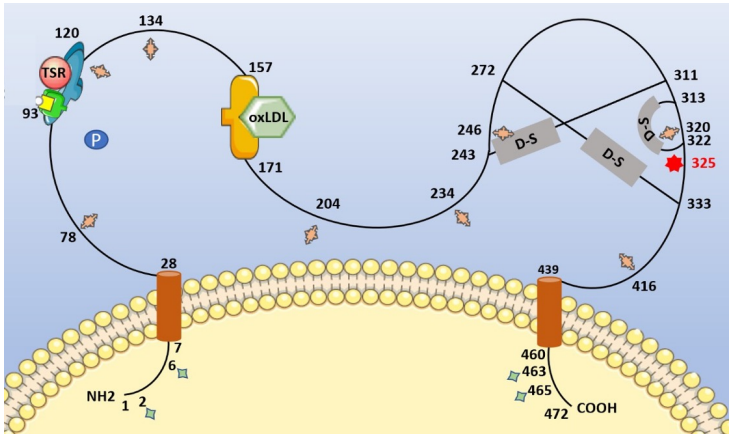

i)

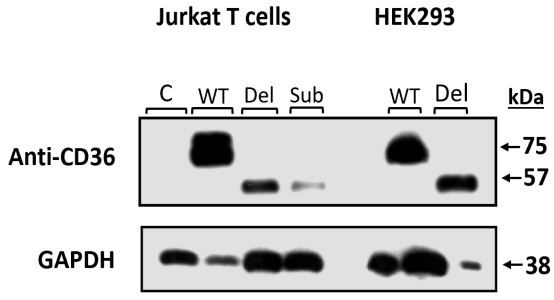

j)

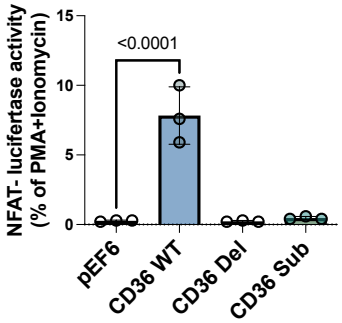

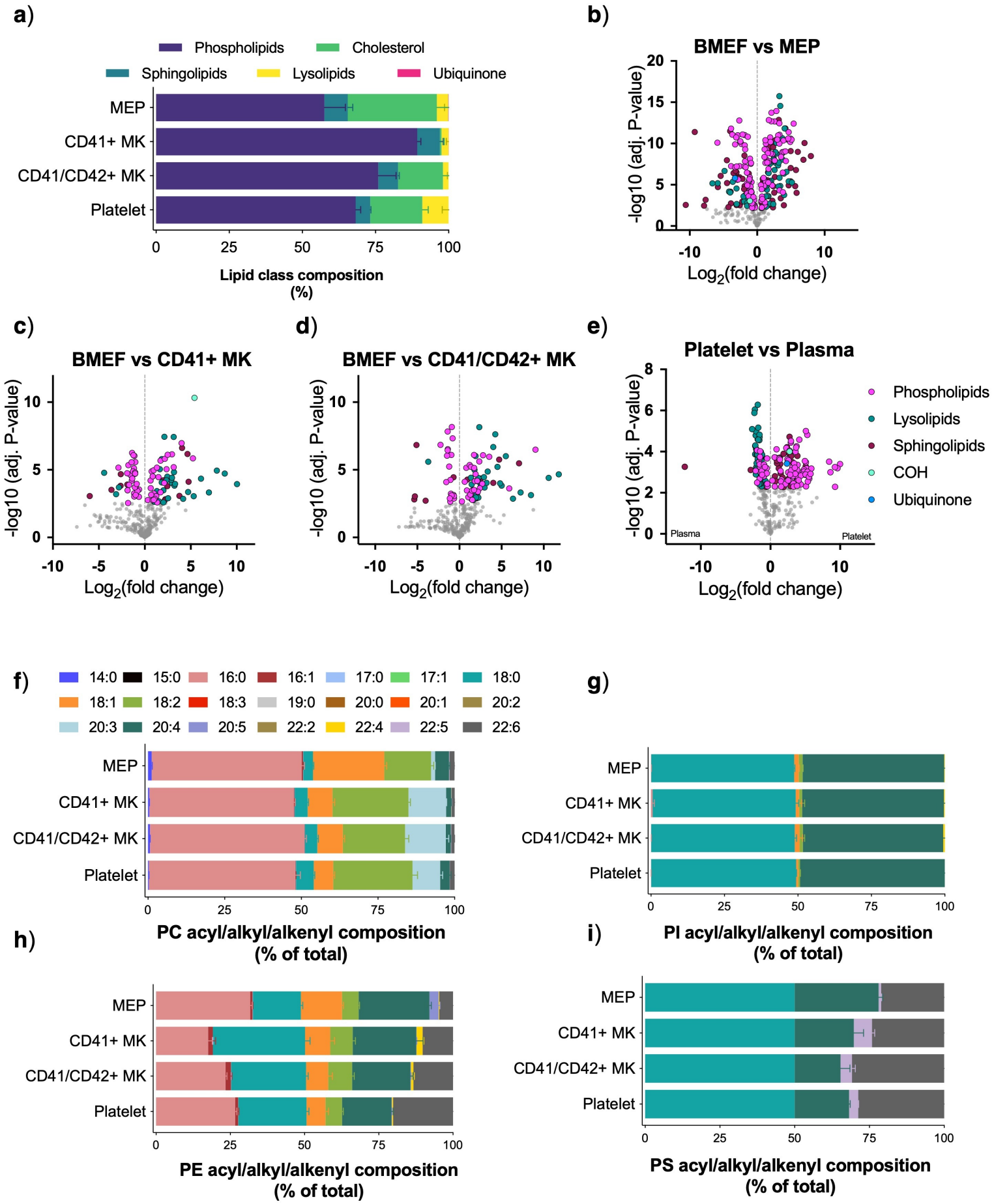

Extended Data Figure 1

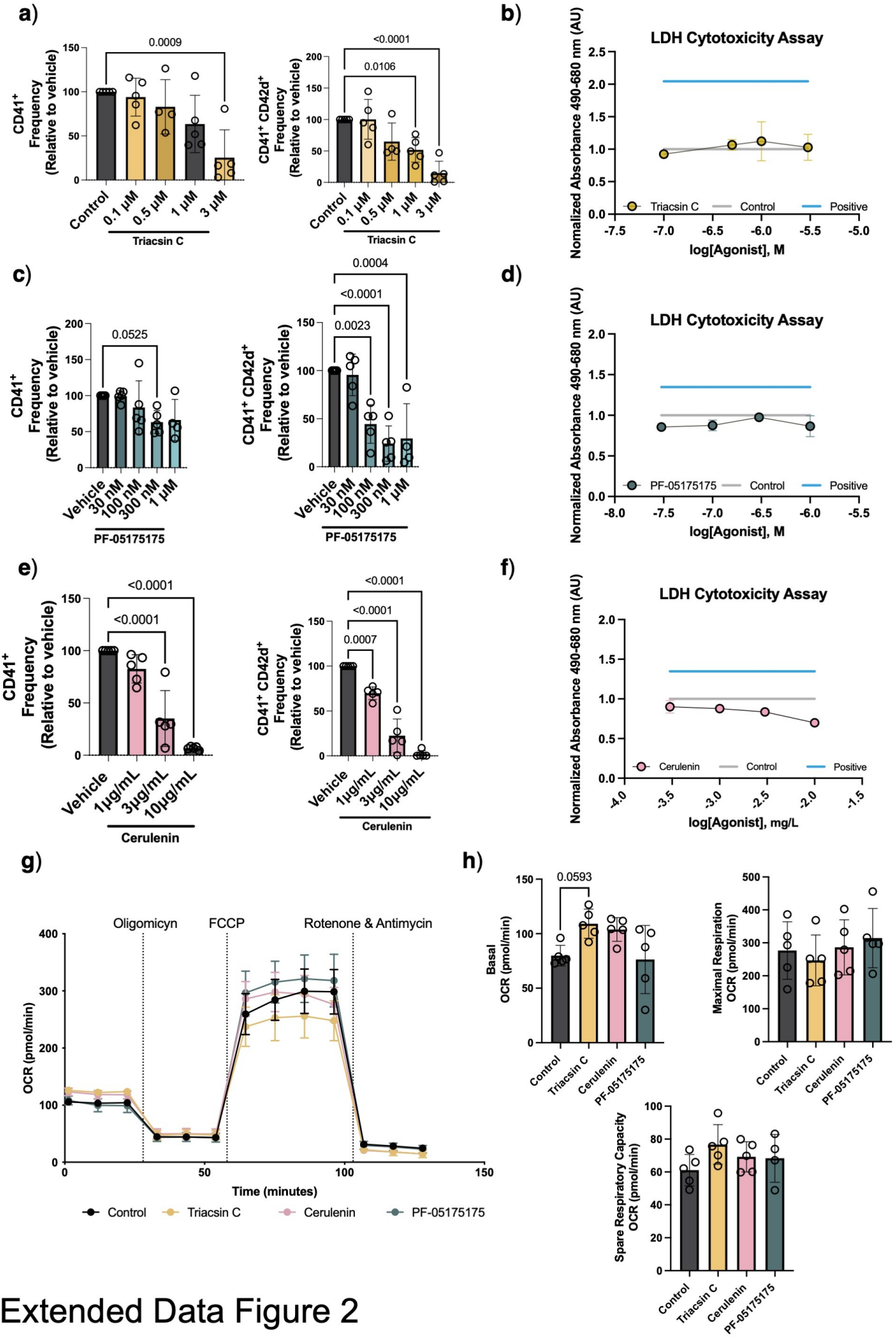

Extended Data Figure 2

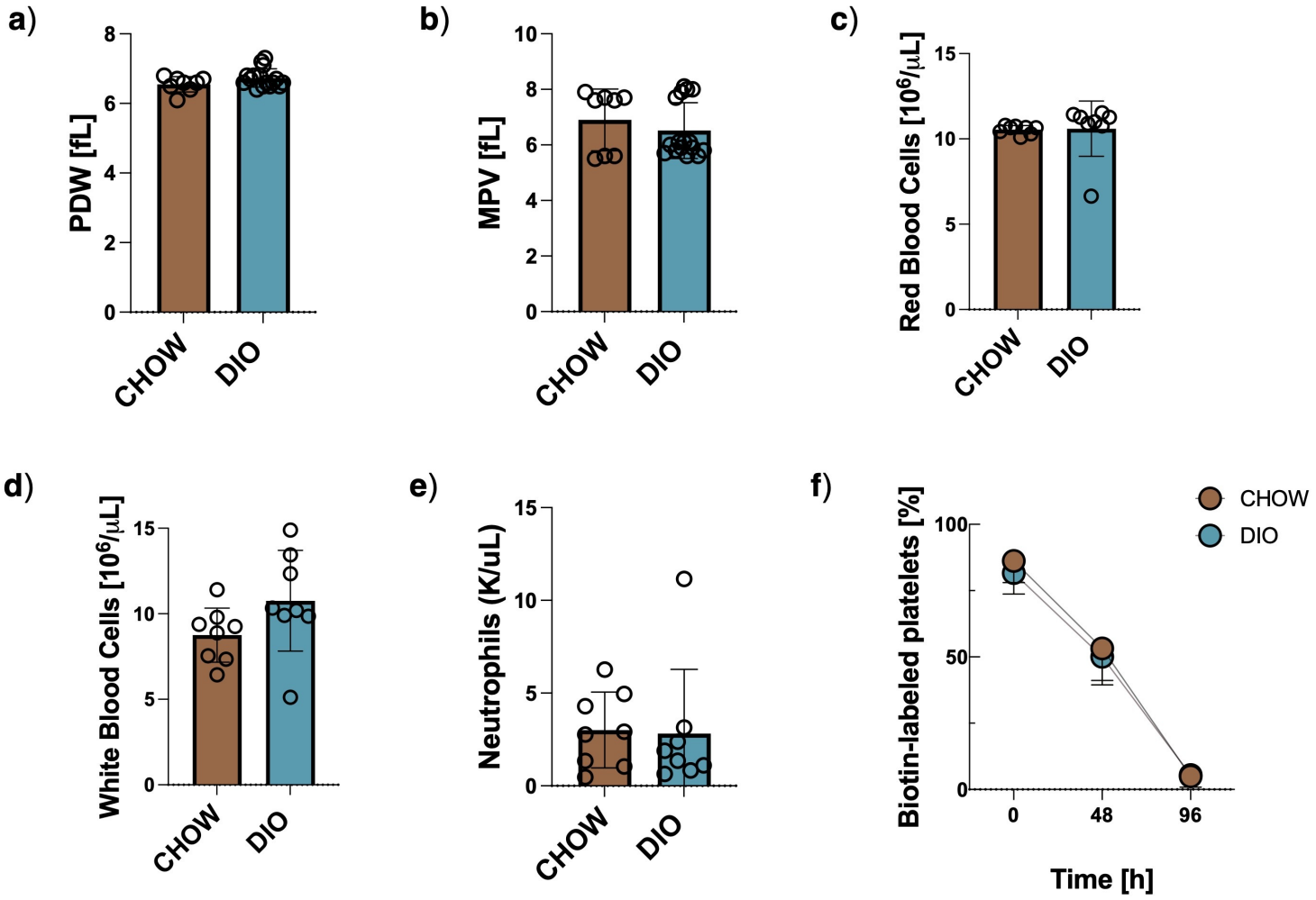

Extended Data Figure 3

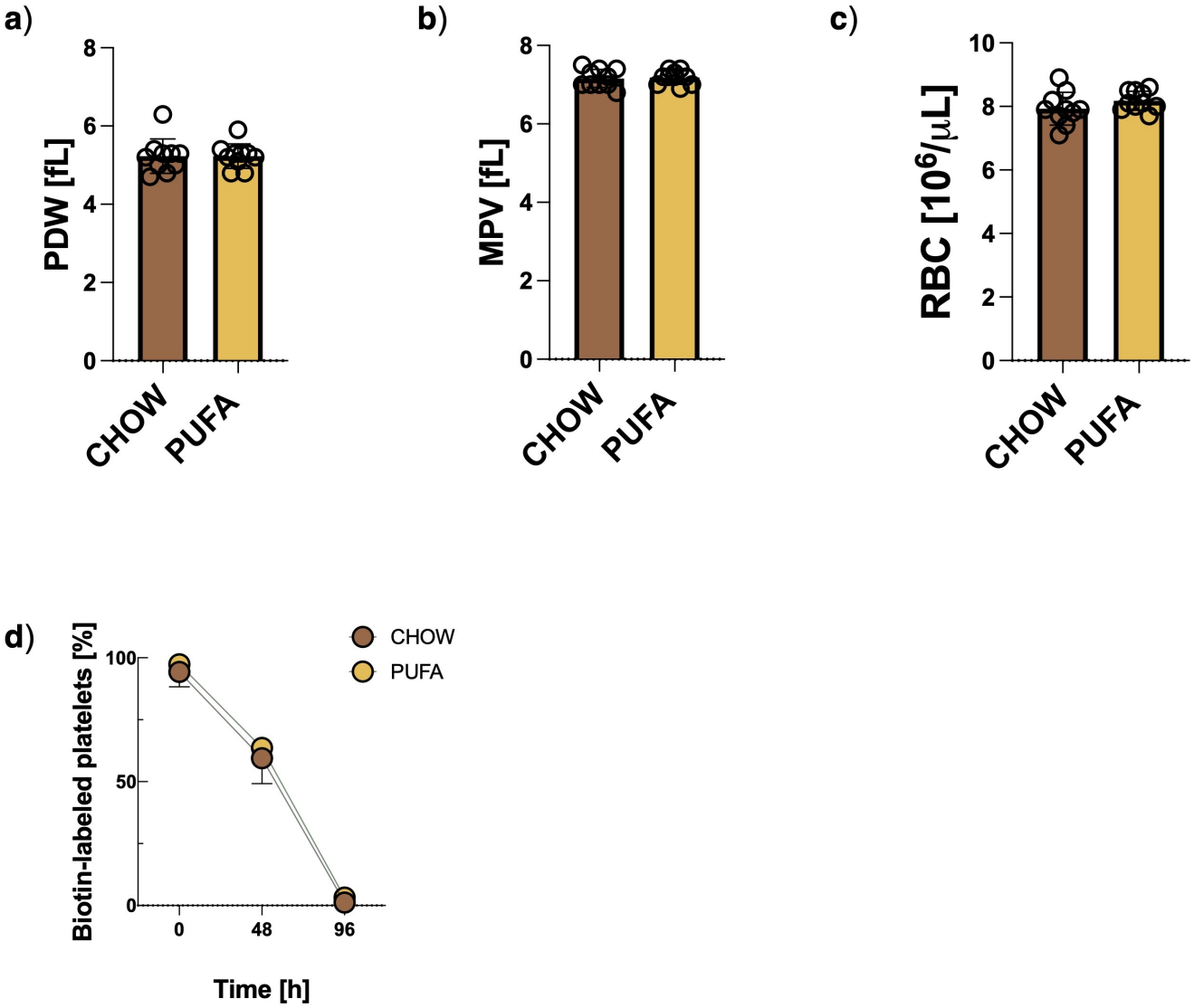

Extended Data Figure 4

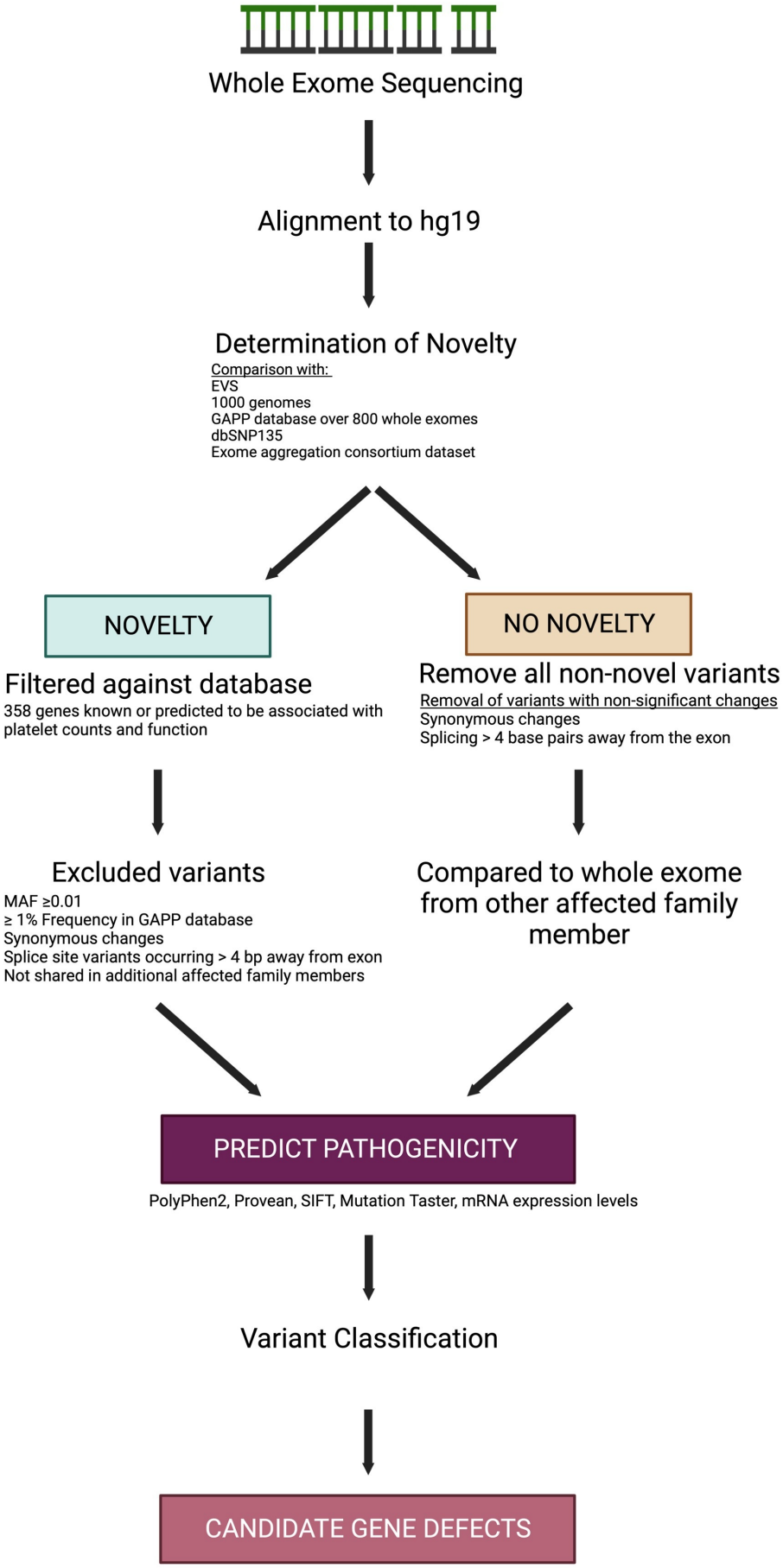

Extended Data Figure 5

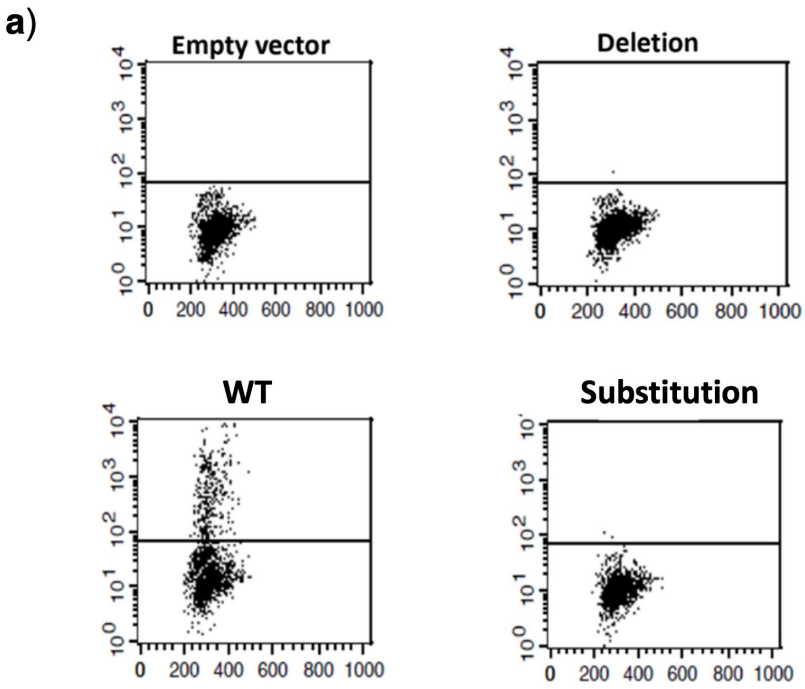

Extended Data Figure 6

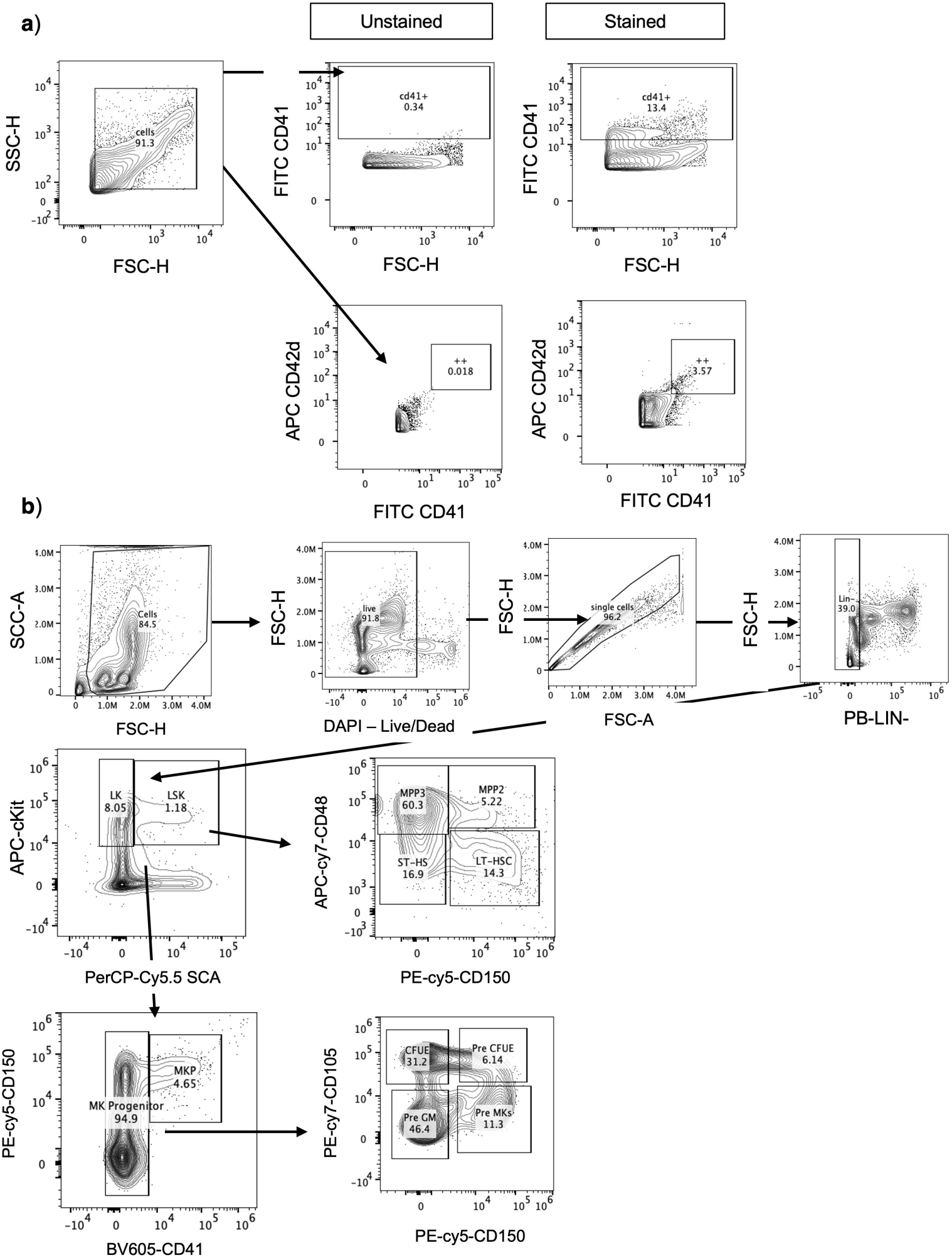

Extended Data Figure 7

Extended Data Table 1. Thrombopoietin measurements in plasma from mice fed with chow, DIO and PUFA-enriched diets

	Normal Range	CHOW	DIO	PUFA
Number of values		4	5	5
Mean TPO [pg/mL]	724-3706	838.4	1007	1416
Std. Deviation		93.82	205.4	190.9

Extended Data Table 2: Summary of variants included in UK-GAPP study.

Patients	5.I	5.II
Total number of variants identified by WES	43,774	43,995
Total number of variants within 358 platelet genes panel	233	243
Total number of variants (excluding synonymous and intronic variants)	149	135
Total number of variants with MAF ≤ 0.01	26	24
Total number of variants after pathogenicity prediction	19	17
Total shared variants	11	11
Plausible candidate variants	1	1